Development of Cable-Adjustable UAV Slung Payload Transportation System

Ahmed Waleed AbdelRahman Etman

A THESIS SUBMITTED TO THE FACULTY OF GRADUATE STUDIES
IN PARTIAL FULFILLMENT OF THE REQUIREMENTS
FOR THE DEGREE OF
MASTER OF SCIENCE

GRADUATE PROGRAM IN
EARTH AND SPACE SCIENCE
YORK UNIVERSITY
TORONTO, ONTARIO

AUGUST 2026

© Ahmed Etman, 2026

Abstract

Unmanned aerial vehicles (UAVs) carrying suspended payloads can support transportation, delivery, inspection, and environmental sampling tasks where landing is unsafe or infeasible. However, payload swing can reduce positioning accuracy, increase collision risk, and affect UAV stability.

This thesis develops a cable-adjustable UAV slung-payload system that enables payload lowering and retrieval while the UAV remains at a safe operating height. Cable length is estimated using an open-loop time-based method, avoiding direct length feedback. Flight data are used to identify the payload natural frequency and damping ratio, and Zero Vibration (ZV) and Zero Vibration and Derivative (ZVD) input shapers are implemented to reduce swing during UAV motion. The system is evaluated through simulation and hardware experiments under nominal and mismatched cable length conditions.

Water sampling is used as a practical validation application integrating cable adjustment, obstacle-aware path planning, swing reduction, and mission execution.

Dedication

To my supervisor, my family, my fiancée and everyone who supported me throughout this work.

Acknowledgements

I would like to express my sincere gratitude to my supervisor, Professor Jinjun Shan, for his guidance, support, and trust throughout my Master's research. I am sincerely thankful for the opportunity he provided to pursue this research and under his mentorship, which has greatly contributed to my academic and professional development.

I would also like to thank my committee member, Professor Regina Lee, for her time, thoughtful feedback, and valuable suggestions, which helped improve the quality and clarity of this thesis.

I am grateful to my lab mates Ali Sherif, Pukun Lu, Amaldev Haridevan, Hunter Schofield, Yida Zang, SyedReza, Hao Zhang, Hao Wang and special thanks for Dr. Junjie Kang for their collaboration, discussions, and support. Working alongside such a dedicated and supportive group made this research both productive and enjoyable, and I appreciate the contributions and encouragement of everyone in the lab.

I would like to express my heartfelt appreciation to my parents, my sisters and my family for their unconditional love, sacrifices, and constant encouragement.

I would also like to extend my heartfelt gratitude to my fiancée Rania for her endless love, patience, encouragement, and support throughout my graduate studies. Her constant belief in me and her presence during both the challenging and rewarding moments of this journey have meant more to me than words can express.

Finally, I would like to thank my friends for their understanding, and encouragement, which helped me maintain balance during my graduate studies.

Table of Contents

Abstract ii

Dedication iii

Acknowledgements iv

Table of Contents v

List of Tables viii

List of Figures ix

Nomenclature xi

1 Introduction 1

1.1 Background and Motivation 1

1.2 Problem Statement 7

1.3 Research Gap 9

1.4 Objectives 10

1.5 Contributions 11

1.6 Thesis Organization 11

2 Literature Review 13

2.1 UAV Slung Payload Transportation 13

2.2 Dynamics and Control of Cable Suspended Payloads 15

2.3 Swing Reduction Methods for Suspended Payloads 18

2.4 Input Shaping for Vibration Suppression 23

2.5 Cable Adjustable Systems 27

2.6 UAV-Based Water Sampling 29
2.7 Summary 31

3 Cable-Adjustable System Design **32**
3.1 System Design Requirements 32
3.2 UAV Platform and Design Constraints 33
3.3 Cable-Adjustment Mechanism 35
3.4 Fabrication and Integration 39
3.5 Cable-Length Adjustment and Estimation 41

4 Input Shaping for Swing Reduction **48**
4.1 Quadrotor Suspended Payload Dynamics 48
4.2 Input Shaper Formulation and Parameterization 50
4.3 Implementation in the UAV Command Architecture 57
4.4 Simulation Evaluation 59
4.4.1 Simulation Setup and Evaluation Metrics 60
4.4.2 Nominal Input Shaping Evaluation 62
4.4.3 Cable-Length Mismatch Evaluation 66
4.4.4 Payload-Mass Variation Evaluation 69
4.4.5 Summary of Simulation Results 72
4.5 Experimental Evaluation 73
4.5.1 Experimental Setup 73
4.5.2 Hardware Input Shaping Test 75
4.5.3 Summary of Experimental Results 78

5 Application: Water Sampling **80**
5.1 Mission-Level Validation Overview 80

5.2 Water Sampling Payload 81
5.3 Obstacle-Aware Mission Planning 82
5.4 Mission Scenario 1 84
5.5 Mission Scenario 2 87
5.6 Mission-Level Results and Discussion 91
5.7 Summary 93

6 Conclusion and Future Work **95**

6.1 Conclusion 95
6.2 Limitations 97
6.3 Future Work 98

Bibliography **99**

List of Tables

3.1 QDrone2 specifications relevant to the cable-adjustment mechanism. . . . 35

3.2 Selected servo motor specifications for the cable-adjustment mechanism. . 38

3.3 Mass breakdown of the cable-adjustment mechanism components. 38

3.4 Mean measured cable-length change from data collection. 43

3.5 Validation results for cable release. 46

3.6 Validation results for cable retraction. 47

4.1 Simulation studies used to evaluate the input shaping method. 60

4.2 Nominal simulation parameters for the input shaping evaluation. 61

4.3 Input shaper parameters used in the nominal simulation case. 61

4.4 Simulation swing-angle metrics for the reference command. 65

4.5 Cable-length mismatch cases used in simulation. 66

4.6 Swing-angle metrics for the cable-length mismatch cases. 68

4.7 Payload-mass variation cases used in simulation. 70

4.8 Swing-angle metrics for the payload-mass variation cases. 71

4.9 Experimental hardware test parameters. 75

4.10 Experimental swing-angle metrics for the hardware input shaping test. . . 77

5.1 Mission points for scenario 1. 84

5.2 Payload swing metrics for mission scenario 1. 87

5.3 Mission points for scenario 2. 89

5.4 Payload swing metrics for mission scenario 2. 91

5.5 Reduction in maximum absolute payload swing angle using ZVD shaping. 92

5.6 Water collection results for the two mission scenarios. 92

List of Figures

1.1 UAV cable-suspended payload system 6

1.2 Representative applications of UAV slung-payload transportation 7

1.3 Water sampling application 7

3.1 QDrone2 quadrotor platform 34

3.2 CAD models of the structural designed components. 36

3.3 CAD design of the cable-adjustment mechanism and its integration with the QDrone2 platform. 37

3.4 Servo Motor. 37

3.5 Cable-adjustment mechanism integrated with the QDrone2 platform: (a) front view and (b) side view. 40

3.6 Data collection and validation set up. 42

3.7 OptiTrack camera system used to measure the UAV and payload vertical positions. 42

3.8 Quadratic fitting of motor command time as a function of cable-length change. 44

4.1 Schematic representation of the quadrotor suspended-payload system . . 49

4.2 Input shaping concept. 52

4.3 Sensitivity curves of ZV and ZVD input shapers 56

4.4 Implementation of the input shaper in the UAV command architecture. . . 58

4.5 Reference commands for the nominal simulation case. 63

4.6 UAV position responses for the nominal simulation case. 64

4.7 Payload swing response θ_x for the nominal simulation case. 65

4.8 Payload swing response θ_y for the nominal simulation case. 65

4.9 Payload swing response θ_x for the cable-length mismatch case $L_a = 0.8$ m. 67

4.10 Payload swing response θ_y for the cable-length mismatch case $L_a = 0.8$ m. 67
4.11 Payload swing response θ_x for the cable-length mismatch case $L_a = 1.2$ m. 68
4.12 Payload swing response θ_y for the cable-length mismatch case $L_a = 1.2$ m. 68
4.13 Effect of payload-mass variation on the maximum swing angle. 70
4.14 Effect of payload-mass variation on the RMS swing angle. 72
4.15 Experimental setup for the UAV suspended-payload input shaping test. . . 74
4.16 Experimental *y*-direction command comparison for the unshaped, ZV shaped, and ZVD shaped cases. 75
4.17 Experimental *y*-position tracking responses for the unshaped, ZV shaped, and ZVD shaped commands. 76
4.18 Experimental payload swing response θ_y for the unshaped, ZV shaped, and ZVD shaped commands. 77
5.1 Designed water sampling payload used for the mission-level validation. . 82
5.2 Physical arena setup for mission scenario 1. 85
5.3 Three-dimensional planner result for mission scenario 1 showing the raw path and reduced waypoint path. 86
5.4 Raw A* path and reduced waypoint path for mission scenario 1. 86
5.5 Physical arena setup for mission scenario 2. 88
5.6 Three-dimensional planner result for mission scenario 2 showing the raw path and reduced waypoint path. 89
5.7 Raw A* path and reduced waypoint path for mission scenario 2. 90

Nomenclature

Acronyms

UAV	Unmanned Aerial Vehicle
ZV	Zero Vibration
ZVD	Zero Vibration and Derivative
PID	Proportional-Integral-Derivative controller
RMS	Root Mean Square
MAE	Mean Absolute Error
P–P	Peak-to-peak value
A*	A-star search algorithm
LOS	Line of sight
CAD	Computer-Aided Design
PLA	Polylactic Acid
PWM	Pulse Width Modulation
QUARC	Real-time control software environment used with the Quanser platform

Symbols

x, y, z	UAV position coordinates in the inertial frame
ϕ	UAV roll angle
θ_{pitch}	UAV pitch angle
ψ	UAV yaw angle
ξ	UAV position vector, $\xi = [x\ y\ z]^T$
q	Outer-loop state vector of the UAV suspended-payload system

u	Generalized input vector
$M_c(q)$	Coupled-system inertia matrix
$V_c(q,\dot{q})\dot{q}$	Coriolis and centrifugal terms of the coupled system
$G(q)$	Gravitational term of the coupled system
g	Gravitational acceleration
m_q	UAV mass
m_p	Payload mass
L	Cable length
L_0	Initial cable length
ΔL	Change in cable length
t_{rel}	Cable-release command duration
t_{ret}	Cable-retraction command duration
d_a	Vertical offset between the UAV COG and the cable attachment point
z_q	Measured UAV vertical position
z_p	Measured payload vertical position
θ_x	Payload swing angle in the x-direction plane
θ_y	Payload swing angle in the y-direction plane
ω_n	Natural frequency of the suspended payload
ω_d	Damped natural frequency of the suspended payload
ζ	Damping ratio
K	Input-shaper damping parameter
T_d	Input-shaper time delay
A_i	Amplitude of the i-th input-shaper impulse
t_i	Time location of the i-th input-shaper impulse
n	Number of impulses in the input shaper
$r(t)$	Original reference command

$r_s(t)$	Shaped reference command
$C(\omega_n, \zeta)$	Cosine component of the residual vibration expression
$S(\omega_n, \zeta)$	Sine component of the residual vibration expression
$V(\omega_n, \zeta)$	Residual vibration magnitude
$\mathbf{p}_0$	Initial mission position
$\mathbf{p}_f$	Final mission position
$\mathbf{w}_i$	i-th mission waypoint
x_i, y_i, z_i	Position coordinates of the i-th waypoint
ψ_i	Yaw command of the i-th waypoint
T_s	Simulation duration
T_e	Evaluation duration

1 Introduction

1.1 Background and Motivation

Unmanned aerial vehicles (UAVs) have become increasingly important robotic platforms for missions that require mobility, rapid deployment, and access to locations that are difficult, unsafe, or inefficient for direct human operation. In addition to their widespread use for sensing, mapping, surveillance, and inspection, UAVs are increasingly being investigated for physical interaction tasks in which the vehicle must transport, lower, retrieve, or deploy a payload. These capabilities are relevant to applications such as search and rescue, infrastructure inspection, delivery, environmental monitoring, and field sampling, where landing may be unsafe, or infeasible. In such cases, suspending the payload below the UAV using a cable provides a practical method for interacting with the environment while maintaining a safe separation between the aerial vehicle and the task location [1][2][3].

Compared with rigidly attached payloads, cable-suspended payloads provide greater flexibility for tasks that require placement or interaction at a distance from the UAV body. Figure 1.1 illustrates UAV cable-suspended payload. A suspended payload can be lowered into narrow, sensitive, or difficult to access regions while the UAV remains above obstacles, uneven terrain, water surfaces, or other hazardous areas. Figure 1.2 shows some representative application scenarios for UAV cable-suspended payload. This is particularly useful when direct landing may damage the vehicle, disturb the environment, or reduce mission safety. For example, in environmental monitoring and water sampling, the UAV can remain above the water surface while a sampling device is lowered to the desired location as shown in Figure 1.3. Similarly, in delivery or deployment tasks, the payload can be positioned near a target without requiring the UAV to land. These advantages make UAV slung payload systems attractive for real-world missions where accessibility, safety,

and operational flexibility are important.

In many UAV payload transportation missions, the payload is not only required to be transported between locations, but also to be deployed, lowered, or retrieved during operation. This capability becomes particularly important in environments where landing is infeasible or unsafe, such as over water surfaces, uneven terrain, confined spaces, obstacle-rich areas, or hazardous regions. A cable-adjustment mechanism enables the UAV to maintain a safe operating altitude while regulating the vertical position of the suspended payload relative to the target location. As a result, tasks such as sample collection, payload placement, and payload recovery can be performed without requiring direct contact between the UAV and the environment. Therefore, cable adjustment expands the functionality of a conventional slung payload system from passive transportation to active payload deployment and environmental interaction.

The use of an adjustable cable introduces the need to estimate or determine the payload cable length during operation. Some aerial suspended-load systems rely on additional sensing, external motion-capture systems, onboard cameras, or vision-inertial estimation to obtain payload position, cable direction, or swing-related states [4][5][6][7]. These approaches can provide valuable state information for feedback control and aggressive maneuvering, but they may also increase system complexity, sensing requirements, calibration effort, and sensitivity to environmental conditions such as occlusion, lighting variation, or reflections. For lightweight field-oriented systems, a simpler implementation may be preferable when the cable mechanism is primarily used for release and retrieval during specific mission phases. In this thesis, cable length is estimated without a dedicated cable-length sensor, reducing hardware complexity while introducing uncertainty that must be considered in swing-reduction design and evaluation.

However, the use of a suspended payload also introduces a significant dynamic challenge. The payload behaves like a pendulum and can oscillate when the UAV accelerates,

decelerates, turns, or tracks a sequence of waypoints. These oscillations can reduce payload positioning accuracy, increase the risk of collision with obstacles, disturb the task environment, and lead to unstable UAV motion. In constrained environments, payload swing is especially problematic because the UAV, cable, and payload must remain within safe regions throughout the mission. A small deviation in payload motion may cause contact with surrounding objects, inaccurate payload placement, or unsafe interaction with the target region. Therefore, swing reduction is a key requirement for reliable UAV slung payload transportation.

The control of UAVs carrying cable-suspended payloads has been widely studied because the coupled UAV payload system is underactuated and exhibits nonlinear behavior. Previous work has addressed trajectory generation, nonlinear control, cooperative transportation, obstacle avoidance, and aggressive flight with suspended loads [8][9][10][11][12]. These studies have demonstrated that careful trajectory planning and control design can significantly improve load behavior. However, many high-performance approaches depend on accurate system models, payload-state feedback, additional sensing, or computationally demanding optimization. While these methods are valuable, their implementation can be challenging on small UAV platforms where payload capacity, power availability, onboard computation, wiring, and sensing complexity are limited.

For practical UAV slung payload systems, reducing sensing and implementation complexity is an important design consideration. Additional sensors for measuring cable length, payload position, or swing angle may increase mass, power consumption, calibration requirements, and mechanical complexity. In field applications, sensing can also be affected by environmental conditions, occlusion, lighting variation, water reflection, or limited visibility. Therefore, there is a need for approaches that improve payload behavior without requiring extensive payload-side instrumentation or complex feedback architectures. Feedforward command shaping is attractive in this context because

it can reduce oscillatory motion by modifying the reference command before it is tracked by the UAV, rather than relying on direct measurement of the payload oscillation during flight.

Input shaping is a feedforward vibration reduction technique originally developed for flexible and lightly damped systems. The basic idea is to design a sequence of delayed and scaled command components such that the vibration caused by one component is cancelled by subsequent components. Classical Zero Vibration (ZV) and Zero Vibration and Derivative (ZVD) input shapers are widely used because of their simple structure and low computational cost. The ZV shaper is designed to cancel vibration at a selected natural frequency, while the ZVD shaper provides increased robustness to modeling errors and frequency mismatch at the cost of a longer command duration [13][14]. These properties make input shaping suitable for UAV slung payload transportation, where the suspended payload has a dominant oscillatory mode and the shaped command can be implemented as a reference filter before the UAV position controller.

Although cable adjustment improves mission capability, it also affects the oscillatory characteristics of the suspended payload. The dominant swing frequency depends on the cable length; therefore, uncertainty in the estimated cable length can lead to uncertainty in the natural frequency used for input shaper design. This issue is particularly important for feedforward methods such as input shaping, which rely on estimates of the natural frequency and damping ratio. As a result, an input shaper designed for one cable length may become less effective when the actual cable length differs from the expected value. This motivates the study of cable-length-dependent swing behavior and the evaluation of input shaper performance under both nominal and mismatched cable length conditions.

In addition to swing reduction, practical slung payload missions require obstacle-aware path planning. Unlike point to point flight in open space, real mission environments may include walls, narrow passages, restricted regions, or task-specific approach constraints.

When a payload is suspended below the UAV, the planned path must consider not only the vehicle motion but also the safety margin required by the cable and payload. Prior studies have shown that trajectory generation for quadrotors with cable-suspended payloads becomes more challenging in obstacle-filled environments because the UAV, cable, and load must all remain within feasible regions [10][12]. Therefore, path planning and swing reduction should be considered together at the mission level to improve safe and repeatable operation in constrained environments.

Water sampling provides a representative real-world application that brings these challenges together. UAV assisted water sampling has been studied as a method for collecting samples from locations that may be difficult, unsafe, or time-consuming to access using conventional manual or boat-based methods [15][16][17]. In such missions, the UAV should transport the sampling device to the target region, avoid obstacles, remain safely above the water surface, lower the payload to collect the sample, and return without excessive payload oscillation. Recent research has also considered multirotor UAVs with cable suspended mechanisms for water sampling and swing-free transportation, further demonstrating the relevance of slung payload systems to this application [18][19].

This thesis is motivated by the need for a practical cable-adjustable UAV slung payload transportation system that can support payload lowering while reducing swing during flight.The proposed work combines cable adjustment mechanism, cable-length estimation, experimentally identified swing characteristics, feedforward input shaping, and obstacle-aware mission execution. Water sampling is adopted as a representative mission-level validation application, as it requires the coordinated integration of payload transportation, cable-based lowering and retrieval, accurate target positioning, obstacle-aware navigation, and safe operation without landing. To evaluate the system at the mission level, the proposed framework is tested in two obstacle-constrained map scenarios with different path requirements. In this way, the thesis addresses the broader problem of UAV slung

payload transportation while using water sampling as a practical application to demonstrate the feasibility and usefulness of the developed system.

The experimental scope of this thesis is limited to a controlled indoor environment and to water sampling as the mission-level validation application. The developed mechanism, cable-length estimation approach, input-shaping implementation, and planning framework are motivated by requirements that can also arise in other suspended-payload tasks; however, the experimental results presented in this thesis should not be interpreted as direct validation for all UAV slung-payload applications or for outdoor operation. Generalization to other payloads, environments, and mission conditions would require additional system-specific evaluation. Accordingly, water sampling is used in this work to demonstrate the integrated framework under the defined experimental conditions rather than to establish universal performance across slung-payload applications.



Figure 1.1: UAV cable-suspended payload [20].

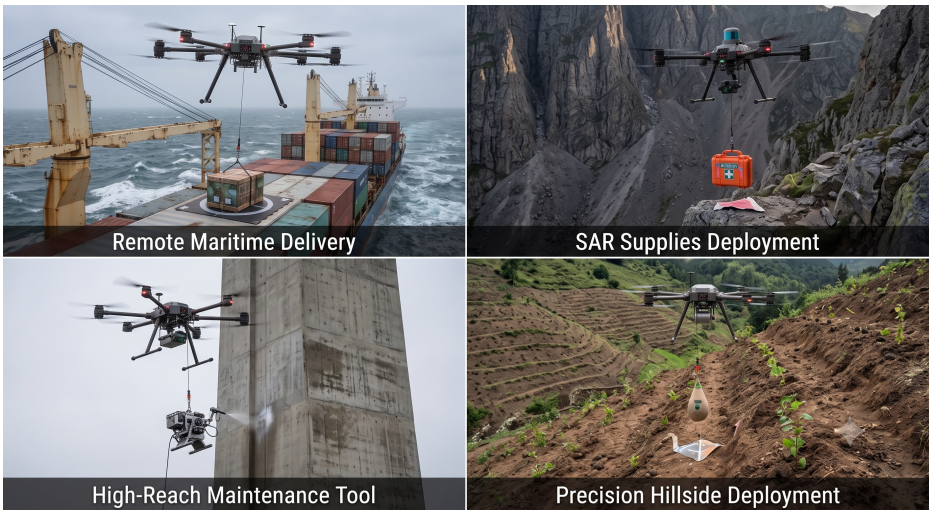

Figure 1.2: Representative applications of UAV cable-suspended payload [20].


Figure 1.3: Water sampling application [21].

1.2 Problem Statement

UAV slung payload transportation provides an effective approach for missions in which a payload must be transported, deployed, lowered, or retrieved without requiring the aerial vehicle to land. However, reliable operation of such systems remains challenging

because payload motion, cable configuration, sensing limitations, and mission constraints are strongly coupled. When the UAV changes speed, changes direction, or follows waypoint-based trajectories, the suspended payload can oscillate relative to the vehicle. These oscillations can reduce payload positioning accuracy, decrease safety margins near obstacles, disturb the task environment, and lead to unstable UAV motion.

The challenge becomes more significant when payload lowering and retrieval are required during the mission. A cable-adjustable mechanism increases the operational capability of the UAV by allowing the payload to interact with a target location while the vehicle remains at a safe altitude. However, this capability introduces the need to determine the cable length with sufficient accuracy, since the oscillatory behavior of the suspended payload depends on the cable configuration. Direct sensing of cable length, payload position, or swing angle can improve state awareness, but it may also increase system mass, hardware complexity, calibration requirements, and integration effort. Therefore, a key research problem is to support cable adjustment and swing reduction while maintaining a practical and lightweight system implementation.

In addition to payload swing and cable adjustment, realistic slung payload missions often require operation in constrained environments. The UAV must reach a target region while avoiding obstacles, maintaining clearance for the suspended payload, and executing task-specific actions such as lowering, sampling, retrieval, and return. In such scenarios, point to point motion in open space is not sufficient. The system must combine feasible path generation with swing-aware transportation so that the UAV and payload can move safely and repeatably through constrained mission layouts. Cable adjustment may also be required to satisfy mission-specific geometric constraints, such as reducing the suspended configuration to pass safely through restricted regions.

Water sampling is considered in this thesis as a representative application of UAV slung payload transportation rather than as an isolated task. The mission requires the UAV

to transport a suspended sampler to a target region, operate in an obstacle-constrained environment, maintain safe distance from the water surface, lower and retrieve the payload, and return safely after completing the task. These requirements make the application useful for evaluating the proposed system at the mission level, since successful execution depends on the combined performance of the cable-adjustment mechanism, swing-reduction method, path planner, and experimental UAV platform.

The central problem addressed in this thesis is how to develop a practical cable-adjustable UAV slung payload transportation system with reduced sensing complexity. The proposed work investigates cable-length estimation without direct cable-length feedback, identifies the swing characteristics of the suspended payload from flight data, and applies feedforward input shaping to reduce payload oscillations during fixed-length flight segments. Simulation studies are used to evaluate the input shaping approach and compare swing reduction performance under different conditions, while indoor hardware experiments validate the method on the UAV slung payload platform. The complete framework is then demonstrated through two obstacle constrained water sampling scenarios that integrate cable adjustment, path planning, swing reduction, and mission execution.

1.3 Research Gap

Although UAV slung payload transportation has been widely studied, much of the existing work focuses on individual aspects of the problem, such as load modeling, trajectory generation, feedback control, or obstacle avoidance. Fewer studies consider the complete system level challenge in which a UAV must transport a suspended payload, adjust the cable length for deployment or retrieval, reduce payload swing with limited sensing, and execute a constrained mission. In particular, many high performance approaches rely on additional payload-state sensing, direct cable or swing measurements, external perception, or complex control structures, which may increase implementation difficulty for UAV

platforms.

The gap addressed in this thesis is the need for a practical cable adjustable UAV slung payload transportation framework that integrates cable adjustment mechanism, cable length estimation, feedforward swing reduction, obstacle aware path planning, and mission-level validation. This gap is especially relevant for applications where the UAV should avoid landing, operate near obstacles, lower and retrieve a payload, and maintain acceptable payload motion during transportation. The thesis addresses this gap by developing a cable-adjustable UAV slung payload system and demonstrating the complete framework through obstacle constrained water sampling missions.

1.4 Objectives

The main objective of this thesis is to develop a cable-adjustable UAV slung payload transportation system. The work focuses on a reduced sensing implementation in which payload lowering and retrieval are achieved using a cable-adjustment mechanism, while payload swing during UAV motion is reduced using feedforward command shaping. The framework is further evaluated through obstacle constrained water sampling missions to demonstrate the integration of payload transportation, cable adjustment, path planning, and swing reduction in a representative real world application.

The specific objectives of this thesis are as follows:

- Design and integrate a cable-adjustable UAV slung-payload system for payload lowering and retrieval.
- Implement and evaluate ZV and ZVD input shaping for suspended-payload swing reduction using the identified payload dynamics.
- Validate the complete framework through obstacle-constrained water sampling scenarios.

1.5 Contributions

The main contributions of this thesis are summarized as follows:

- A cable-adjustment mechanism is designed, fabricated, and integrated with the UAV slung-payload platform. A command-based cable-length adjustment and estimation method is developed using experimentally calibrated relationships between the desired cable-length change and motor command duration. The approach enables payload lowering and retrieval without requiring direct cable-length feedback.
- Zero Vibration (ZV) and Zero Vibration and Derivative (ZVD) input-shaping methods are implemented within the UAV position-command architecture for suspended-payload swing reduction. The shaper parameters are determined from the suspended-payload vibration characteristics, and their performance is evaluated through nominal, cable-length-mismatch, and payload-mass-variation simulations. Hardware experiments further validate the swing-reduction performance for the tested fixed cable configuration.
- The developed cable-adjustment, command-based cable-length estimation, swing-reduction, and obstacle-aware path planning are integrated into a complete UAV suspended-payload mission framework. The integrated system is experimentally validated through two constrained indoor water sampling scenarios that require payload transportation, cable adjustment, obstacle avoidance, payload lowering and retrieval, and water collection.

1.6 Thesis Organization

The remainder of this thesis is organized as follows. Chapter 2 reviews the related literature on UAV suspended-payload transportation, payload swing reduction methods, input

shaping, cable-adjustable payload systems, and UAV-based water sampling applications. Chapter 3 presents the design, fabrication, and integration of the cable-adjustment mechanism on the QDrone2 platform, followed by the command-based cable-length estimation method used for release and retraction. Chapter 4 develops the input-shaping approach used for suspended-payload swing reduction, including the suspended-payload model, ZV and ZVD shaper design, simulation evaluation, and hardware validation. Chapter 5 presents water sampling validation of the complete system, including obstacle-aware path generation, waypoint reduction, and hardware mission tests in two constrained scenarios. Finally, Chapter 6 summarizes the main findings of the thesis and discusses possible directions for future work.

2 Literature Review

2.1 UAV Slung Payload Transportation

UAV slung payload transportation refers to the use of aerial vehicles to carry a payload suspended below the vehicle by a cable or tether. This configuration extends the role of UAVs from sensing and observation platforms to systems capable of physically transporting, deploying, and retrieving objects. Such capability is relevant to applications where direct landing is not feasible, safe, or necessary, including search and rescue, field deployment, delivery, infrastructure inspection, and environmental monitoring. Bernard et al. demonstrated autonomous transportation and deployment of loads using aerial robots for search and rescue missions, showing that UAVs can be used not only for observation but also for delivering useful payloads to target locations [1]. Similarly, Michael et al. investigated cooperative manipulation and transportation using multiple aerial robots connected to a payload through cables, highlighting the potential of cable based aerial transportation for three dimensional payload manipulation [2].

Cable suspended payload transportation offers advantages compared with rigidly attaching the payload to the UAV body. A suspended payload can be positioned below the vehicle, allowing the UAV to maintain clearance from terrain, water surfaces, structures, or hazardous regions while the payload interacts with the target environment. This separation can improve operational flexibility in missions where the vehicle should avoid landing or where the payload must be placed at a location different from the UAV body position. In cooperative aerial transportation, cables also allow multiple UAVs to share the load and manipulate larger or more complex payloads while maintaining feasible vehicle configurations [2][22].

Despite these advantages, slung payload transportation introduces important challenges that are not present in conventional UAV flight with rigidly attached payloads. The

suspended load can oscillate relative to the UAV, and its motion is coupled with the vehicle motion through the cable. As a result, acceleration, deceleration, turning, and trajectory tracking can excite payload swing. This affects payload positioning accuracy, increases the difficulty of trajectory generation, and can reduce the safety margin during operation near obstacles or target regions. Sreenath et al. modeled and controlled a quadrotor with a cable suspended load as a differentially flat hybrid system, demonstrating that the load dynamics must be considered when generating feasible trajectories for accurate transportation [8].

Recent studies have continued to investigate UAV slung payload transportation as a coupled underactuated motion control and planning problem. For example, trajectory-generation methods have been studied to reduce payload vibration during quadrotor transportation [23]. Path invariant and path following controllers have also been developed to regulate the motion of quadrotors with cable-suspended payloads along prescribed paths while accounting for the coupled UAV–payload dynamics [24][25]. Other recent work has proposed control frameworks for stabilizing UAV slung payload systems and planning control frameworks for autonomous payload transportation in constrained environments [26][27]. These studies show that slung payload transportation remains an active research area involving trajectory design, control, planning, and experimental validation.

The literature on UAV suspended load transportation includes both single-UAV and multi-UAV systems. Single-UAV systems are attractive because of their simpler coordination requirements and lower platform complexity, but they are limited by the payload capacity and the underactuated nature of the vehicle load system. Multi-UAV systems can increase load capacity and improve payload manipulation authority, but they introduce additional challenges related to formation control, cable tension distribution, inter vehicle coordination, and communication. Recent review studies of aerial transportation with suspended cable payloads have emphasized that these systems are nonlinear, underactuated,

and sensitive to cable and load modeling assumptions, making practical implementation and experimental validation important parts of the research field [3].

Overall, UAV slung payload transportation provides a flexible approach for aerial delivery, deployment, and environmental interaction tasks. However, the benefits of cable suspended payloads are accompanied by challenges related to payload oscillation, coupled UAV–load dynamics, sensing requirements, and mission feasibility in constrained environments. These challenges motivate further study of suspended load dynamics, swing reduction, cable configuration, and planning methods, which are reviewed in the following subsections.

2.2 Dynamics and Control of Cable Suspended Payloads

The dynamics of UAVs carrying cable suspended payloads are more complex than those of conventional UAVs with rigidly attached payloads. In a slung payload configuration, the UAV and the payload are dynamically coupled through the cable, and the payload motion depends on the translational acceleration of the aerial vehicle, gravity, cable tension, and cable geometry. Even when the payload is modeled as a point mass and the cable is assumed to be massless and rigid, the resulting system is nonlinear and underactuated. This underactuation occurs because the UAV thrust and attitude are directly controlled, while the payload motion is indirectly influenced through the motion of the suspension point. As a result, trajectory tracking and payload positioning require careful consideration of both vehicle and load dynamics.

Several studies have formulated suspended load UAV systems using nonlinear dynamic models. Sreenath et al. modeled a quadrotor with a cable suspended load as a differentially flat hybrid system and demonstrated that the load dynamics must be included when generating feasible trajectories for payload transportation [8]. In related work, Sreenath, Lee, and Kumar developed a coordinate free dynamic model on the configuration space of the

quadrotor and cable direction, and used geometric control to address the nonlinear nature of the quadrotor load system [28]. These studies show that suspended load transportation cannot be treated as simple point to point UAV motion, since payload swing and cable direction are part of the system dynamics.

Lagrange based modeling has also been widely used to derive the equations of motion for quadrotor transportation systems. Liang et al. presented a nonlinear hierarchical control framework for an unmanned quadrotor transportation system using a full dynamic model that includes the quadrotor position and the projected payload swing angles [29]. Their formulation describes the outer-loop dynamics in terms of inertia, Coriolis and centripetal, gravity, and input terms, while the inner-loop dynamics describe the quadrotor attitude motion. This type of formulation is useful because it explicitly shows the coupling between quadrotor translation and payload swing, as well as the underactuated nature of the overall transportation system.

More recent work has continued to address the nonlinear and underactuated nature of UAV slung payload systems using path based, cascade control, adaptive control, and motion control formulations. Akhtar et al. developed path-invariant and path-following controllers for quadrotors carrying cable-suspended payloads, where the payload is regulated along prescribed geometric paths while considering the coupled vehicle–payload dynamics [24][25]. Kang et al. proposed a control framework for UAV slung payload transportation that stabilizes both the UAV motion and the tether swing angles [26]. Further developments have considered adaptive control and virtual nonholonomic constraint based motion control for underactuated UAV slung payload systems, highlighting the continued importance of stabilizing the unactuated payload swing dynamics during transportation [30][31].

Control strategies for cable suspended payload systems have also been developed using nonlinear and geometric control methods. Geometric control approaches are attractive

because they represent the system directly on nonlinear configuration manifolds, including the special Euclidean group, the special orthogonal group, and the unit sphere, rather than relying only on local angle parameterizations. This formulation helps avoid singularities that can arise from Euler angle representations. These methods have been applied to both single-UAV and cooperative multi-UAV load transportation problems, where the objective is to track a desired payload trajectory while maintaining stable cable and vehicle motion [22][28]. Although such approaches provide strong theoretical properties, they generally require accurate dynamic models and sufficient state information about the UAV, payload, and cable configuration.

The cable model itself also affects the complexity of the control problem. Many suspended load studies assume a rigid, massless cable with a fixed length, which simplifies the dynamics and makes the payload behave approximately as a pendulum attached to the UAV. However, this assumption may be insufficient when cable flexibility, cable mass, large deformation, or variable cable length must be considered. Goodarzi et al. developed a coordinate free dynamic model for a quadrotor transporting a payload connected through a flexible cable, where the cable was represented as a serial connection of links [32]. This type of modeling provides a more detailed description of cable behavior, but it also increases the dimensionality and complexity of the control problem.

Trajectory generation and control have also been used to reduce swing and improve suspended load transportation performance. Palunko et al. proposed trajectory generation for swing free maneuvers of a quadrotor with a suspended payload using a dynamic programming approach [9]. Tang and Kumar formulated trajectory generation for a quadrotor with a cable suspended payload as a mixed integer quadratic program, allowing obstacle avoidance and payload constraints to be included in the planning problem [10]. Foehn et al. further considered fast trajectory optimization for agile quadrotor maneuvers with a cable suspended payload, showing the importance of planning trajectories that

respect the coupled quadrotor load dynamics [11]. More recent trajectory and planning control methods have extended this direction by incorporating vibration reduction, nonlinear model predictive control, and autonomous payload transportation in constrained environments [23][33][27]. These studies demonstrate that load aware trajectory generation can improve transportation performance, but they may also require detailed models, optimization routines, and accurate knowledge of the system state.

In summary, previous research has established strong modeling and control foundations for UAVs carrying cable suspended payloads. The literature shows that suspended load systems are nonlinear, underactuated, and sensitive to cable and payload assumptions. Advanced nonlinear control, geometric control, adaptive control, path following control, and trajectory optimization methods can improve load transportation performance, but practical implementation may require accurate models, additional sensing, and increased computational complexity. These observations motivate the review of swing reduction methods in the next subsection, including approaches that can reduce payload oscillation through trajectory design, feedback control, or feedforward command modification.

2.3 Swing Reduction Methods for Suspended Payloads

Payload swing reduction is a central problem in UAV slung-payload transportation because the suspended load can oscillate when the UAV accelerates, decelerates, changes direction, or tracks a sequence of waypoints. These oscillations can reduce payload positioning accuracy, increase the risk of collision, and limit the repeatability and safety of transportation and deployment tasks. The literature has addressed this problem through several main approaches, including trajectory planning, trajectory optimization, feedback control, nonlinear and geometric control, perception-based control, feedforward command modification, and learning-based methods. Each approach offers different advantages, but also introduces practical challenges related to modeling accuracy, sensing requirements,

computational cost, robustness, and experimental implementation.

One common approach is to design trajectories that inherently reduce the excitation of payload oscillations. Palunko et al. proposed a dynamic programming method for generating swing free maneuvers of a quadrotor with a suspended payload [9]. This approach showed that the UAV trajectory can be planned to reduce residual payload oscillation rather than relying only on feedback correction after swing has already been excited. Faust et al. further investigated learning swing free trajectories for UAVs with suspended loads, where trajectory generation was treated as a learning problem to reduce residual oscillations [34]. These trajectory based methods are useful because they address swing reduction at the reference generation level. However, their performance can depend strongly on the accuracy of the assumed model, the operating conditions used for planning, and the ability of the physical UAV to track the planned trajectory accurately.

Optimization based trajectory generation has also been widely investigated for suspended load UAV systems. Tang and Kumar formulated trajectory generation for a quadrotor with a cable suspended payload as a mixed integer quadratic programming problem, allowing obstacle avoidance and payload constraints to be incorporated into the planning process [10]. Foehn et al. considered fast trajectory optimization for agile quadrotor maneuvers with a cable suspended payload, demonstrating the potential of optimization based planning for aggressive suspended load motion [11]. Zeng et al. later used direct collocation with a differential flatness based hybrid model to generate dynamically feasible paths for a quadrotor with a cable suspended payload [12]. More recent planning control frameworks have further incorporated nonlinear model predictive control, whole body safety constraints, and online trajectory generation for autonomous UAV payload transportation [27][33]. These methods can produce high performance trajectories under complex constraints, but they may require detailed system models, careful parameter tuning, and significant computation. In addition, planned trajectories may become less ef-

fective when the actual payload mass, cable length, damping, or environmental conditions differ from the assumptions used during planning.

Another class of swing reduction methods modifies the smoothness and frequency content of the reference trajectory. Instead of solving a full optimal control problem, these methods design reference profiles that reduce the vibration transmitted from the UAV to the suspended payload. Alkomy and Shan investigated the vibration reduction of a quadrotor with a cable suspended payload using polynomial trajectories and analyzed how different polynomial trajectory profiles affect payload vibration [23]. Such methods are attractive because they connect the trajectory shape directly to the oscillatory response of the suspended payload. However, trajectory smoothing approaches may increase mission duration or reduce maneuver aggressiveness, and their effectiveness still depends on the relationship between the trajectory time scale and the payload natural dynamics.

Feedback control methods reduce swing by using measured or estimated system states during flight. These approaches can improve disturbance rejection and robustness compared with purely planned motion, especially when the payload is perturbed or when the model does not perfectly match the physical system. Nicotra et al. proposed a nested saturation controller for a UAV carrying a suspended load, with the objective of steering the aerial robot to a desired reference while limiting payload sway [35]. Guerrero et al. developed a passivity based control approach for a quadrotor transporting a cable suspended payload with minimum swing [36]. Guerrero Sánchez et al. also considered swing attenuation for a quadrotor transporting a cable suspended payload using an Euler–Lagrange model and a control strategy aimed at safe and fast transportation [37]. More recent feedback control studies have addressed swing suppression using cascade control, continuous sliding mode control, adaptive control, virtual nonholonomic constraints, disturbance estimation, and active disturbance rejection control [26][38][30][31][39][40]. These feedback approaches can provide stronger robustness to disturbances, but they

typically require payload swing information, cable direction, or reliable state estimation. Their implementation may therefore depend on motion capture, vision systems, inertial sensing, observers, or additional payload side instrumentation.

Nonlinear and geometric control methods have also been used to address the coupled and underactuated nature of suspended load transportation. Sreenath, Lee, and Kumar developed geometric control and differential flatness tools for a quadrotor with a cable suspended load [28]. Liang et al. proposed a nonlinear hierarchical controller that separates the outer-loop position and payload swing dynamics from the inner-loop attitude dynamics, demonstrating experimentally that payload swing can be suppressed while maintaining quadrotor positioning accuracy [29]. Goodarzi et al. considered geometric control for a quadrotor transporting a payload connected through a flexible cable, showing how more detailed cable modeling can be incorporated into the control design [32]. Path invariant and path following control methods have also been developed to regulate the motion of quadrotors with cable suspended payloads along prescribed geometric paths while accounting for the coupled UAV–payload dynamics [24][25]. These methods provide strong theoretical foundations and can handle nonlinear system behavior, but they often require accurate dynamic models, full or partial knowledge of payload states, and careful controller implementation. The complexity increases further when cable flexibility, large angle motion, multi-UAV cooperation, or variable cable configurations are considered.

Perception based and model predictive control approaches have been introduced to address suspended load control when payload states must be estimated using onboard sensors. Tang et al. demonstrated aggressive flight with suspended payloads using vision based control, showing that vision can be used to estimate payload motion and close the loop on the load behavior [4]. Li et al. proposed a perception constrained model predictive control framework for quadrotors with suspended loads using a monocular

camera and an inertial measurement unit, combining state estimation, prediction, actuator constraints, and camera field of view constraints [5]. Li et al. also proposed a complete planning and control framework for autonomous UAV payload transportation, combining real time planning with adaptive nonlinear model predictive control to address constrained environments and model uncertainty [27]. These approaches are important for moving beyond external motion capture environments. However, they also introduce challenges related to camera calibration, payload visibility, lighting variation, occlusion, image processing reliability, and onboard computation. In constrained or reflective environments, such as near water surfaces, perception based methods may require additional robustness considerations.

Feedforward command modification represents another approach to swing reduction. In this category, the reference command is shaped before being tracked by the UAV so that the resulting motion reduces excitation of the dominant oscillatory mode of the suspended payload. Command shaping methods have been applied to quadrotor and UAV systems carrying suspended or slung payloads, including command shaping for quadcopters with suspended loads, robust command shaping for quadrotor slung systems with varying parameters, and trajectory planning approaches that incorporate input shaping actions for suspended payload transportation [41][42][43]. For these systems, feedforward methods are relevant because the suspended payload often exhibits a dominant pendulum-like mode during fixed-length transportation.However, feedforward swing reduction depends on the accuracy of the estimated vibration parameters, especially the natural frequency and damping ratio. Variations in cable length, payload mass, damping, or actuator response can therefore reduce shaping performance. For this reason, command shaping methods are reviewed separately in the next subsection, with specific attention to their robustness properties and their suitability for cable length dependent payload dynamics.

Learning based methods have also been explored for suspended load manipulation

and trajectory generation. Palunko et al. proposed a reinforcement learning approach for autonomous suspended load manipulation using aerial robots [44]. Learning based methods can be useful when the system dynamics are difficult to model accurately or when the desired behavior must be learned from interaction or data. However, they introduce challenges related to training data requirements, convergence, generalization to unseen payload configurations, safety during exploration, and interpretability. For safety critical UAV transportation missions, learned policies often require careful validation before experimental deployment, especially when the payload can swing near obstacles or sensitive target regions.

Overall, the literature shows that suspended payload swing reduction can be approached through planning, optimization, feedback control, nonlinear control, perception based control, feedforward control, and learning. Trajectory and optimization methods can reduce swing by designing load-aware reference motion, but they may be sensitive to modeling assumptions and computational requirements. Feedback and nonlinear control methods can improve disturbance rejection, but they usually require accurate payload state information and more complex implementation. Perception based methods reduce reliance on external motion capture, but they introduce sensing and visibility constraints. Feedforward control methods provide a model based way to reduce excitation of payload oscillation, but their performance depends on the accuracy of the vibration parameters. These challenges motivate a closer review of input shaping as a vibration suppression method for suspended payload transportation.

2.4 Input Shaping for Vibration Suppression

Input shaping is a model based feedforward command design method used to reduce residual vibration in lightly damped dynamic systems. The main idea is to modify a reference command before it is applied to the system so that the vibration induced by one

part of the command is cancelled by the vibration induced by later parts of the command. Singer and Seering introduced command preshaping as a method for reducing endpoint vibration by altering the desired input command [13]. Since then, command shaping has been applied to a wide range of flexible and oscillatory systems, including cranes, robotic manipulators, flexible structures, spacecraft, and aerial systems [14]. For UAV slung payload transportation, input shaping is relevant because the suspended payload often exhibits a dominant pendulum-like swing mode during fixed-length flight segments.

Classical input shapers are usually designed using estimates of the system natural frequency and damping ratio. The Zero Vibration (ZV) shaper is designed to eliminate vibration at a selected frequency for a nominal model, while the Zero Vibration and Derivative (ZVD) shaper adds robustness by making the residual vibration less sensitive to small errors in the assumed natural frequency [13][14]. This robustness is especially important for suspended payload systems because the dominant swing frequency depends on the cable length and may vary with payload configuration, damping, and operating conditions. However, increased robustness is generally obtained at the cost of a longer shaped command duration, which can affect maneuver time and trajectory timing. Therefore, the choice of shaper involves a tradeoff between vibration suppression, robustness to modeling uncertainty, and command execution time.

Input shaping has been investigated in aerial suspended load systems, especially for helicopter and UAV slung load applications. Potter et al. applied input shaping to reduce the swing of a model helicopter sling load and showed that shaped commands can reduce load oscillations during lateral motion [45]. Adams et al. combined input shaping with model following control for a helicopter carrying a suspended load, demonstrating that feedforward shaping can be integrated with feedback control architectures for improved tracking and swing reduction [46]. Potter et al. also presented a planar experimental remote controlled helicopter testbed with a suspended load, where adding input shaping to the

controller reduced maximum and residual load swing during repositioning maneuvers [47]. These studies are important because they show that command shaping is not limited to industrial cranes or flexible manipulators, but can also be applied to aerial systems with suspended payload dynamics.

Input shaping has also been considered for multirotor UAVs carrying suspended loads. Homolka et al. reported input shaping solutions for drones with suspended payloads, demonstrating the feasibility of augmenting the feedforward path of a multirotor control system with command shapers [48]. Fielding and Nahon developed input shaped trajectory generation and controller design for a quadrotor slung load system, showing how shaped trajectories can be used to reduce payload swing during quadrotor transportation [49]. Huo et al. proposed a vibration elimination method for a quadrotor slung system based on input shaping and double closed-loop control [50]. More recent work has also studied robust command shaping for quadrotor slung systems with varying parameters and sequence constrained trajectory planning that encourages the use of input shaping actions for quadrotor suspended payload transportation [42][43]. Ogunbodede and Singh further investigated load-vibration mitigation for UAVs with cable suspended loads and compared trajectory based vibration reduction with feedback and input shaping prefilter approaches [51].

Although input shaping has been experimentally investigated in aerial slung load systems, the available experimental studies are more limited than the broader simulation and model based literature. Experimental validation has been reported for model helicopter slung load systems, whereas several multirotor suspended load studies present input shaping results mainly through modeling and simulation. This indicates that hardware validation remains an important step when evaluating input shaping for practical UAV slung payload transportation, particularly when the system includes cable length dependent dynamics, actuator limitations, and uncertainty in the suspended load parameters.

A key advantage of input shaping in suspended load systems is that it acts at the

command level. Instead of directly controlling the payload swing angle, the shaped reference reduces the excitation of the payload's dominant oscillatory mode before significant residual vibration is generated. This makes input shaping compatible with existing UAV position control architectures, since the shaped trajectory can be applied as a reference modification before the lower level controller tracks the command. In this sense, input shaping can complement feedback controllers, trajectory generators, and mission planners by reducing the oscillatory content of the commanded motion without requiring direct payload swing feedback in its basic implementation.

The performance of input shaping depends on the accuracy of the vibration model used for shaper design. In UAV slung payload systems, this is closely related to cable length because the natural frequency of the suspended load varies with the effective cable length. Errors in the estimated natural frequency, damping ratio, actuator response, or trajectory timing can reduce the effectiveness of the shaper and may leave residual oscillations after the maneuver. These limitations have motivated robust shaper designs, such as ZVD and higher order shapers, as well as experimental evaluations under parameter mismatch. For cable adjustable suspended load systems, this issue becomes particularly important because the cable length may change between mission phases, and the shaper parameters must correspond to the fixed cable configuration used during each transportation segment.

Overall, input shaping provides a systematic feedforward framework for reducing vibration in systems with dominant oscillatory modes. In UAV slung payload transportation, it is especially relevant for reducing payload swing during fixed-length flight segments. Compared with feedback based swing suppression approaches, input shaping can be implemented as a reference command modification and does not require direct payload position feedback or an additional payload side sensor in its basic form. However, its effectiveness depends on accurate identification or estimation of the suspended load dynamics, and its robustness must be evaluated when cable length, payload mass, damping, or actuator

behavior differ from the nominal design assumptions. These characteristics make input shaping suitable for further investigation in this thesis for cable suspended payload systems, particularly when combined with experimental identification and validation under nominal and mismatched cable length conditions.

2.5 Cable Adjustable Systems

Cable adjustment is an important capability for UAV suspended payload systems when the payload must interact with a target location while the aerial vehicle maintains a safe operating distance. In applications such as water sampling, environmental monitoring, payload delivery, and retrieval, a fixed cable length can limit the ability of the payload to reach the desired interaction point without requiring the UAV to descend close to the surface or obstacle region. For this reason, several UAV suspended payload systems have incorporated dedicated cable adjustment, winch based, or deployable mechanisms to support payload lowering, retrieval, and improved transportation capability [52][53][54][55][56].

Previous work has explored cable adjustable mechanisms for UAV transportation and aerial manipulation beyond application specific sampling systems. Li et al. proposed a variable aerial cable towed system in which multiple UAVs are connected to a payload through cables whose lengths are actively adjusted using embedded winches [52]. This configuration increases the geometric versatility of multi-UAV transportation systems and allows the payload pose to be controlled more flexibly. Yang et al. studied modeling, trajectory planning, and anti swing control for a quadrotor suspended payload system with variable cable length, showing that cable length variation can be incorporated directly into the suspended load control problem [53]. Sarkisov et al. proposed a cable suspended aerial manipulator with winch based actuation, where multiple winch controlled suspension cables are used to modify the system configuration and support whole body control of the aerial manipulation system [54]. Li et al. later investigated quadrotor based suspended

load transportation with active cable length control, showing that variable cable length can improve transportation performance compared with constant length suspended load systems [55]. Goodarzi presented a quadrotor payload-delivery system with a length-varying cable, where the cable length is changed to support payload delivery while the controller stabilizes the quadrotor–payload system [57]. Variable cable length systems have also been studied from a modeling and anti swing control perspective, where the cable length is treated as an additional control related variable in the coupled UAV–payload dynamics [56].

Although these works demonstrate the potential of adjustable cable mechanisms, they also show that such systems often require additional actuators, winches, sensing, calibration, and control complexity. In multi-UAV or multi-cable systems, the mechanism can further increase platform size, coordination requirements, and implementation cost.

Cable adjustable systems also require some form of cable length or deployment state awareness. In previous systems, this information may be obtained from the actuation mechanism, such as spool or winch motion, or indirectly from sensing and estimation of the payload or sampling device. Additional sensors, encoders, cameras, or external tracking systems can improve state awareness, but they may also increase system weight, wiring complexity, calibration requirements, and environmental sensitivity. These issues are especially relevant for small UAV platforms and water related applications, where payload capacity, waterproofing, and reliability are major design constraints.

Overall, the literature shows that cable adjustable and deployable payload mechanisms are valuable for UAV applications that require environmental interaction without landing. However, previous designs often involve tradeoffs between mission capability, mechanism weight, sensing requirements, cost, robustness, and integration complexity. This motivates the development of cable adjustable suspended payload systems with practical cable length awareness and reduced sensing requirements. In this thesis, cable adjustment is

used primarily to support mission-level functionality, such as lowering and retrieving the payload, while swing reduction is applied during fixed-length flight segments using feedforward input shaping.

2.6 UAV-Based Water Sampling

UAV-based water sampling has become an important application for aerial robotics because it allows samples to be collected from locations that may be difficult, unsafe, or time-consuming to access using manual or boat based methods. From a robotics perspective, water sampling is not only an environmental monitoring task, but also a payload transportation and deployment problem. The UAV must transport a sampling device to a target region, maintain safe separation from the water surface, position the payload accurately, collect the sample, and return after completing the task. Therefore, water sampling provides a practical application in which UAV transportation, payload deployment, positioning accuracy, and operational safety must be considered together.

Several studies have demonstrated the feasibility of UAV-assisted water sampling and monitoring. Ore et al. developed an aerial water sampling system capable of collecting multiple small samples during flight [58]. Koparan et al. evaluated a UAV-assisted water-sampling system and showed that UAV-based sampling can provide a safer and more flexible alternative for collecting samples from large or difficult-to-access water bodies [15]. Ryu investigated a UAS-based platform for real time water-quality monitoring, sampling, and visualization, showing the potential of integrating sensing, sampling, and data visualization into a single aerial platform [16]. Zhang et al. also developed a multi rotor UAV system for water quality sampling and multi parameter monitoring, further demonstrating the relevance of UAVs for environmental sampling tasks [17].

For suspended payload UAV systems, water sampling is especially relevant because the sampling device can be lowered toward the water while the UAV remains above the

surface. This configuration reduces the need for the aerial vehicle to approach the water directly and can improve operational safety when compared with approaches that require close surface interaction. Panetsos et al. presented a precise position control framework for a multirotor UAV with a cable suspended mechanism during water sampling [18]. In later work, Panetsos et al. developed an end to end motion control framework for autonomous water sampling and swing free transportation using a UAV with a cable suspended mechanism [19]. These studies show that cable suspended sampling is a meaningful application of UAV slung payload transportation, but they also highlight the importance of controlling payload motion during the sampling task.

Water sampling is also a useful mission-level validation scenario because it requires several capabilities to operate together. The UAV must transport the payload, reach the sampling region, maintain sufficient positioning accuracy, reduce suspended load swing, deploy and retrieve the sampling device, and complete the mission safely. In realistic environments, the UAV may also need to navigate around obstacles or follow constrained paths before reaching the target region. When a suspended payload is present, this mission becomes more demanding because payload motion and clearance must be considered in addition to the UAV trajectory.

Overall, the literature shows that UAV-based water sampling is a practical and important application of aerial payload transportation. Existing systems have demonstrated different sampling mechanisms and control strategies, but the task remains challenging because it combines payload transportation, deployment, positioning, environmental interaction, and safe mission execution. This makes water sampling a suitable application for validating a complete cable adjustable UAV slung payload framework that integrates payload transportation, cable adjustment, swing reduction, and constrained mission execution.

2.7 Summary

The reviewed literature shows that UAV slung payload transportation is a useful approach for missions requiring payload transportation, deployment, lowering, or retrieval without landing the aerial vehicle. Previous studies have established strong foundations in suspended load modeling, trajectory generation, nonlinear and geometric control, perception based control, cooperative transportation, and swing reduction. However, suspended payload systems remain challenging because the payload introduces coupled UAV load dynamics, oscillatory motion, sensing requirements, and mission-level constraints that are not present in conventional UAV flight.

The literature also shows that cable adjustable suspended payload systems and UAV water sampling applications are important extensions of this research area. Cable adjustment expands the capability of UAV slung payload systems by enabling payload lowering and retrieval, but it also introduces practical design and sensing challenges such as mechanism weight, actuation complexity, power consumption, and cable length awareness. Water sampling is a useful mission level validation application because it combines payload transportation, cable adjustment, positioning, swing reduction, and safe task execution in one representative scenario.

Based on the reviewed work, there remains a need for an integrated and experimentally validated UAV slung payload framework that combines lightweight cable adjustment, reduced sensing cable length awareness, feedforward swing reduction, and mission-level validation. This thesis addresses this need by developing a cable adjustable UAV slung payload system, estimating cable length without direct cable length feedback, applying input shaping for swing reduction, evaluating performance under nominal and mismatched cable length conditions, and validating the complete framework through a suspended payload water sampling mission.

3 Cable-Adjustable System Design

3.1 System Design Requirements

The cable-adjustment mechanism was designed to extend a UAV slung payload system from fixed-length transportation to a payload-lowering and retrieval system. The main objective was to allow the suspended payload to move vertically with respect to the UAV while keeping the aerial vehicle at a safe operating height. This capability is important for missions in which the payload must interact with a target region below the UAV, such as water sampling, delivery, or deployment tasks, without requiring the UAV itself to land or fly very close to the surface.

Several design requirements were considered during the development of the mechanism. First, the mechanism had to be lightweight and compact so that it could be integrated with the UAV without significantly reducing flight stability or available payload capacity. Since the UAV already carries a suspended load, any additional mass from the motor, spool, mount, and support structure must be minimized. The mechanism also had to be mechanically secure and positioned so that it would not interfere with the propellers, motion-capture markers, or normal operation of the vehicle.

Second, the mechanism had to be integrated using the existing UAV platform as much as possible. The design was required to operate without adding an external battery or a separate onboard electronic system for the cable-adjustment mechanism. This requirement helps reduce added weight, wiring complexity, and integration effort, while keeping the system practical for small UAV implementation.

Third, the mechanism had to provide repeatable cable release and retraction. The cable length must be adjustable during mission phases such as payload lowering and retrieval, while remaining fixed during translational flight segments. This distinction is important because payload swing reduction is applied during flight at a fixed cable

length, whereas cable adjustment is used to change the payload position before or after transportation phases. Therefore, the mechanism must support both cable adjustment and stable fixed-length payload transportation.

Fourth, the mechanism was intended to provide cable length adjustments rather than closed-loop regulation of an exact payload depth. The water-sampling application considered in this thesis requires the sampling payload to be lowered sufficiently into the water and subsequently retrieved, but does not require the payload to track a prescribed submerged depth with centimeter-level accuracy. Accordingly, no fixed cable-length accuracy threshold was imposed a priori. Instead, the achievable adjustment accuracy is quantified experimentally in Section 3.5, and its suitability is interpreted with respect to the mission requirements considered in this work.

Finally, the system was designed to operate without a direct cable-length sensor. Instead of adding an encoder or external cable-length measurement device, the system should estimate the cable length using the known initial cable length and the commanded operation of the cable-adjustment motor. This reduced-sensing requirement helps keep the mechanism simple and lightweight, but it also requires the release and retraction behavior to be repeatable enough for practical cable-length estimation.

3.2 UAV Platform and Design Constraints

The aerial platform used in this work is the QDrone2 quadrotor [59]. The platform provides the flight, sensing, and control infrastructure for the cable-adjustable suspended payload system. Since the cable-adjustment mechanism is integrated directly with the UAV, the platform characteristics impose important design constraints on the mechanical structure, actuation method, wiring, added mass, and available mounting space. Figure 3.1 shows the QDrone2 platform and selected onboard components relevant to the proposed integration.



Figure 3.1: QDrone2 quadrotor platform [59].

The QDrone2 includes onboard sensing and computing components such as an NVIDIA Jetson Xavier NX SOM, multiple RGB cameras, and expandable I/O. These components support indoor flight operation, perception, and experimental integration. In this work, the UAV is operated in an indoor laboratory environment using the Quanser/QUARC real-time control framework, while the vehicle motion is measured using an external motion-capture system.

From a mechanism design perspective, the QDrone2 platform imposes several practical constraints. First, the added cable-adjustment mechanism must be lightweight because the UAV will carry a suspended payload, and any additional mass reduces the available payload margin and can affect flight performance. Second, the mechanism must be compact and mechanically secure so that it does not interfere with the normal vehicle operation. Third, the mechanism must be integrated using the available platform interfaces without requiring an external battery or a separate onboard electronic system. This requirement reduces the added mass, wiring complexity, and implementation effort.

The available I/O and onboard control infrastructure are therefore important for the proposed design. The cable-adjustment actuator must be commanded through the existing UAV control framework, and the mechanism must be compatible with the available power

and signal interfaces. This integration requirement influenced the selection of a compact motor, mounting structure, and command based cable length estimation method. The main platform characteristics relevant to the mechanism design are summarized in Table 3.1.

Table 3.1: QDrone2 specifications relevant to the cable-adjustment mechanism.

Platform	QDrone2 specification
UAV mass	1.6 kg
Maximum payload capacity	300 g
Available PWM channels	2 channels, PWM 4 and PWM 5
PWM output level	3.3 V
Available actuator supply	5 V, maximum 5 A
Control environment	Quanser/QUARC Simulink framework

These platform constraints define the design boundary for the cable-adjustment mechanism. The mechanism must provide cable release and retraction while remaining lightweight, compact, electrically compatible with the UAV platform, and suitable for repeatable suspended-payload experiments.

3.3 Cable-Adjustment Mechanism

The cable-adjustment mechanism was designed as a lightweight UAV integrated actuation system for controlled cable release and retraction. The design combines a continuous-rotation servo motor, a spool, a cable guide, and 3D-printed structural components into a compact assembly that can be mounted below the QDrone2 platform while satisfying mass, power, mounting, and landing-clearance constraints. The mechanism was designed in SolidWorks, with attention to mounting constraints on the UAV frame, cable routing, ground clearance, and the location of the cable contact point relative to the UAV center of gravity.

The motor drives the spool to wind or unwind the cable. The spool is attached directly to the servo shaft, and the cable is routed through a cable guide located below the spool. The purpose of the cable guide is to constrain the cable path during release and retraction

and reduce the possibility of the cable moving laterally outside the spool. The main structural parts were fabricated from PLA because it provides a suitable balance between low mass, ease of fabrication, and sufficient stiffness for the intended experimental operation.

The structural designed components for the cable-adjustment mechanism are shown in Figure 3.2. These components include the landing leg, motor mount, and cable guide, which were designed to support the mechanical integration of the cable-adjustable payload system with the UAV platform.

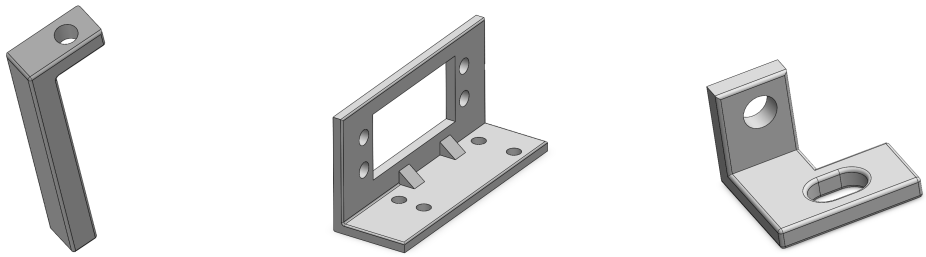

(a) Landing leg (b) Motor mount (c) Cable guide

Figure 3.2: CAD models of the structural designed components.

Figure 3.3 shows the CAD design of the mechanism and its assembled configuration with the QDrone2 platform. The front and side views show the relative placement of the motor, spool, cable guide, and cable path. The assembled views show the mechanism placement below the UAV body and the extended landing legs used to provide clearance for safe takeoff and landing.

The actuator was selected based on the mechanical and electrical constraints of the UAV platform. A continuous-rotation servo motor was preferred over a positional servo because the cable length must be adjusted over multiple spool rotations rather than within a limited angular range. The selected actuator was the INJORA INJS022-360 continuous-rotation servo motor shown in Figure 3.4. This motor provides continuous 360-degree rotation, PWM command compatibility, sufficient torque for cable winding and unwinding,



(a) Front view

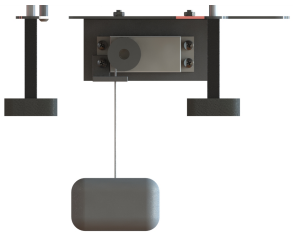

(b) Side view



(c) Assembled view with QDrone2

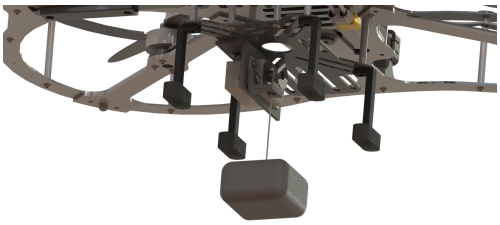

(d) Assembled view (2)

Figure 3.3: CAD design of the cable-adjustment mechanism and its integration with the QDrone2 platform.

and operation within the available 5 V power interface. Therefore, it can be integrated with the UAV without requiring an external battery or a separate onboard electronic system.



Figure 3.4: Servo Motor.

Table 3.2 summarizes the selected servo motor specifications used for the cable-adjustment mechanism.

The motor mount was designed as an L-shaped bracket to support the servo below the UAV body. The mount has dimensions of 70 mm $\times$ 25 mm $\times$ 30 mm with a thickness of 3 mm. The spool has a diameter of 19 mm and a height of 11 mm, and it is mounted on the servo output shaft to convert motor rotation into cable-length change. The nylon cable was selected because it is lightweight and flexible while providing sufficient strength for the suspended payload.

Table 3.2: Selected servo motor specifications for the cable-adjustment mechanism.

Motor specification	Selected motor information
Motor model	INJORA INJS022-360
Motor type	Continuous-rotation digital servo
Operating voltage range	4.8–6.0 V
Rated torque	17 kg·cm
Rotational speed	56 RPM at 4.8 V
Motor dimensions	40 mm × 20 mm × 28 mm
Motor mass	47.7 g
Command signal	PWM
PWM period	20 ms
Neutral command	1500 μs
Max CW command	500 μs
Max CCW command	2500 μs

Since the mechanism is installed below the UAV body, four extended PLA landing legs were added to the UAV frame. Each extended leg has a height of 5 cm and a mass of 1.4 g. These legs provide ground clearance for the motor, spool, and cable guide during takeoff and landing without modifying the main UAV structure.

Table 3.3 summarizes the mass distribution of the main mechanism components. The total added mechanism mass, excluding the cable and small fasteners, is approximately 64.2 g when using the measured component masses.

Table 3.3: Mass breakdown of the cable-adjustment mechanism components.

Component	Quantity	Mass
Continuous-rotation servo motor	1	47.7 g
Spool	1	2.5 g
3D-printed motor mount	1	7.4 g
3D-printed cable guide	1	1.0 g
Extended PLA landing legs	4	5.6 g
Total added mechanism mass	–	64.2 g

The final design satisfies the main platform level constraints by keeping the mechanism compact, lightweight, and compatible with the available UAV power and control command interfaces. The mechanism provides the cable release and retraction motion, the cable

guide improves cable routing consistency, and the extended landing legs provide the required ground clearance for safe operation with the mechanism mounted below the UAV.

3.4 Fabrication and Integration

After completing the CAD design, the custom structural components of the cable-adjustment mechanism were fabricated using additive manufacturing. The motor mount, cable guide, and extended landing legs were printed using PLA material. The parts were printed using a Creality CR-10S Pro 3D printer with a layer height of 0.2 mm, an infill density of 30%, and a nozzle temperature of 190°C.

The assembly process began by mounting the continuous-rotation servo motor to the motor bracket. The spool was then fixed to the servo output shaft so that motor rotation could be converted directly into cable winding and unwinding. The nylon cable was wound around the spool and routed through the cable guide to maintain a consistent cable path below the UAV body. The cable guide was aligned with the spool to reduce lateral cable motion and to help prevent the cable from leaving the spool during release and retraction.

The assembled mechanism was installed below the QDrone2 frame while considering the location of the cable path relative to the UAV body. The mounting location was selected to keep the cable contact point close to the vertical axis passing through the UAV center of gravity, reducing the introduction of unnecessary static moments during suspended-payload operation. The extended landing legs were attached to the UAV frame to provide the required ground clearance for the motor, spool, cable guide, and suspended cable during takeoff and landing. Figure 3.5 shows the real hardware implementation of the cable-adjustment mechanism mounted on the QDrone2 platform.

The electrical integration was completed using the existing UAV platform interfaces. The servo motor was commanded through the available PWM interface and powered

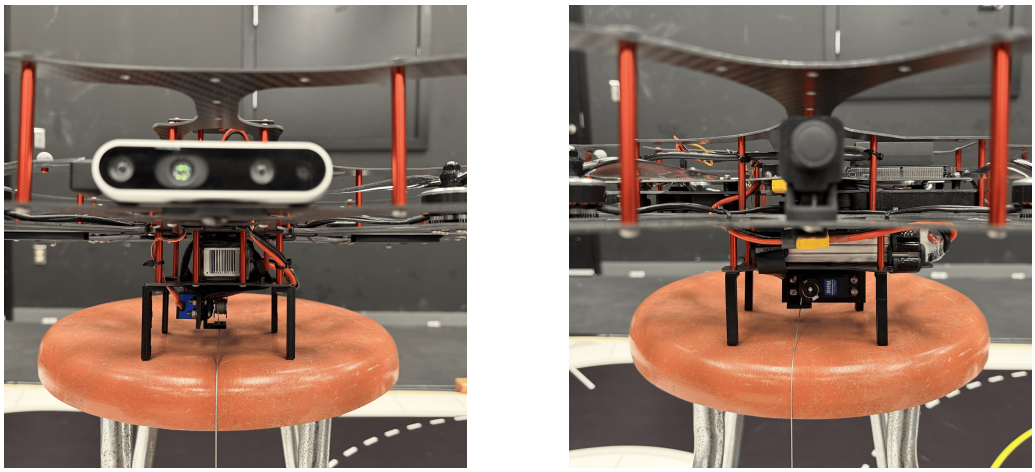

(a) Front view (b) Side view

Figure 3.5: Cable-adjustment mechanism integrated with the QDrone2 platform: (a) front view and (b) side view.

through the available platform supply, avoiding the need for an external battery or an additional onboard electronic unit. The wiring was routed along the UAV frame to reduce interference with the propellers, onboard sensors, and motion-capture markers. This integration approach kept the added hardware compact and reduced the complexity of the experimental setup.

Basic functional tests were conducted after assembly to verify cable release and retraction, motor command response, and load-holding capability. The motor was tested using commands generated from the MATLAB/Simulink environment through the UAV interface. A load test was also conducted using the maximum payload capacity considered for the platform, confirming that the selected motor could hold the payload while drawing a measured current of approximately 0.36 A. These tests verified that the fabricated mechanism was suitable for subsequent cable-length calibration and suspended-payload flight experiments.

3.5 Cable-Length Adjustment and Estimation

The cable-adjustment mechanism is operated without a direct cable-length sensor. Instead, cable-length adjustment is performed using a command based method in which a desired target cable length is converted into a motor command duration through experimentally identified relationships. The initial cable length is known before operation, and the commanded change in cable length is used to update the cable-length value used by the system. Therefore, the cable length is not measured directly during operation; rather, it is inferred from the known initial length, the commanded target length, and the experimentally validated actuation accuracy.

The method was developed using data collections that relate motor command duration to the resulting change in cable length. A data collection setup was prepared by suspending the QDrone2 from the ceiling while the payload was attached to the cable-adjustment mechanism, as shown in Fig. 3.6. This configuration allowed the release and retraction behavior of the cable to be tested safely without flight motion. The UAV and payload vertical positions were measured using the OptiTrack motion-capture system [60][61], shown in Fig. 3.7. Since the payload was suspended below the UAV during data collection, the cable length was obtained from the relative vertical position between the UAV and the payload.

The measured cable length was calculated from the vertical separation between the cable attachment point and the payload. Since the cable attachment point is located $d_a = 0.07$ m below the UAV center of gravity, the measured cable length is expressed as

$$L_{\text{meas}}(t) = (z_q(t) - d_a) - z_p(t), \tag{3.1}$$

where $z_q(t)$ is the measured UAV vertical position, $z_p(t)$ is the measured payload vertical position, and d_a is the vertical offset between the UAV center of gravity and the cable at-

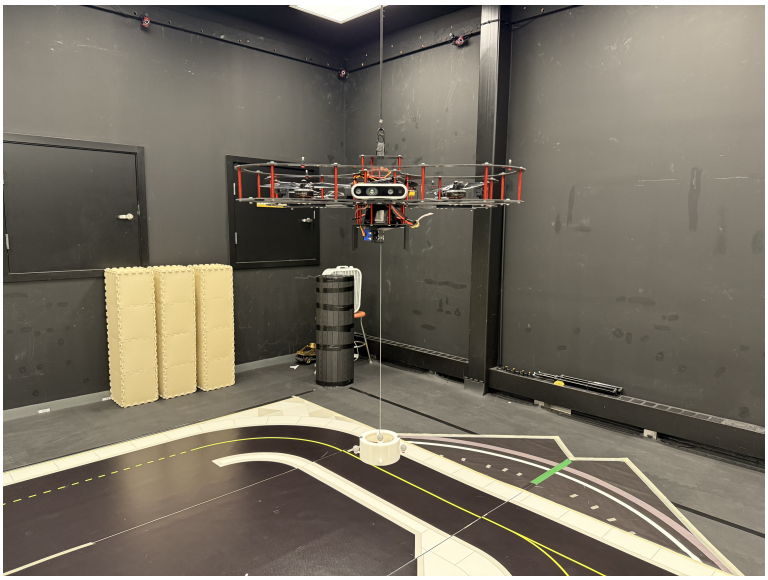

Figure 3.6: Data collection and validation set up.



Figure 3.7: OptiTrack camera system used to measure the UAV and payload vertical positions.

tachment point. The measured change in cable length during each test was then calculated as

$$\Delta L_{\text{meas}} = \left| L_{\text{meas}}(t_f) - L_{\text{meas}}(t_0) \right|, \tag{3.2}$$

where t_0 and t_f are the initial and final times of the motor command.

For data collection, the motor was commanded at a fixed max speed in both release and retraction directions. Command durations from 1 s to 20 s were tested, and each command duration was repeated 10 times for each direction. This resulted in a total of 400 calibration samples. For each command duration, the average cable-length change

was calculated from the 10 repeated trials. Table 3.4 summarizes the mean measured cable-length change for both release and retraction.

The averaged collected data were fitted in MATLAB using a second-order polynomial relationship between the required command time and the desired cable-length change. This form was selected because, during operation, the desired cable-length change is known first, and the required motor command duration must then be computed. Therefore, the fitted relationship is expressed as $t = f(\Delta L)$, where ΔL is the desired cable-length change in millimeters.

Table 3.4: Mean measured cable-length change from data collection.

Command time (s)	Releasing ΔL (mm)	Retracting ΔL (mm)
1	34.9	34.8
2	66.5	65.9
3	105.2	100.6
4	131.6	130.3
5	165.4	164.1
6	211.0	210.7
7	245.7	243.4
8	284.4	281.8
9	328.1	323.5
10	363.1	358.2
11	399.7	393.2
12	427.0	419.5
13	454.5	447.1
14	481.7	472.1
15	518.6	508.0
16	564.2	555.7
17	594.7	587.6
18	630.5	624.0
19	663.3	657.8
20	695.8	686.7

For the release direction, the fitted relationship is

$$t_{\text{rel}} = \left(2.561 \times 10^{-6}\right) \Delta L^2 + 0.0266 \Delta L + 0.2338, \tag{3.3}$$

and for the retraction direction, the fitted relationship is

$$t_{\text{ret}} = \left(2.111 \times 10^{-6}\right) \Delta L^2 + 0.0274 \Delta L + 0.1945, \tag{3.4}$$

where t_{rel} and t_{ret} are the motor command durations in seconds, and ΔL is the desired cable-length change in millimeters. The polynomial relationship is used as an empirical command mapping rather than as a physical model of the system. A second-order form was selected to represent the small nonlinear variation observed over the tested cable-length range while retaining a compact relationship that can be evaluated directly during operation. The objective is not to obtain an exact representation of the cable deployment dynamics, but to determine a practical motor command duration for a requested cable-length change. Consequently, the usefulness of the calibration is assessed using the independent cable-length validation experiments presented below, rather than from the curve fit alone. Figure 3.8 shows the quadratic fits for both release and retraction.

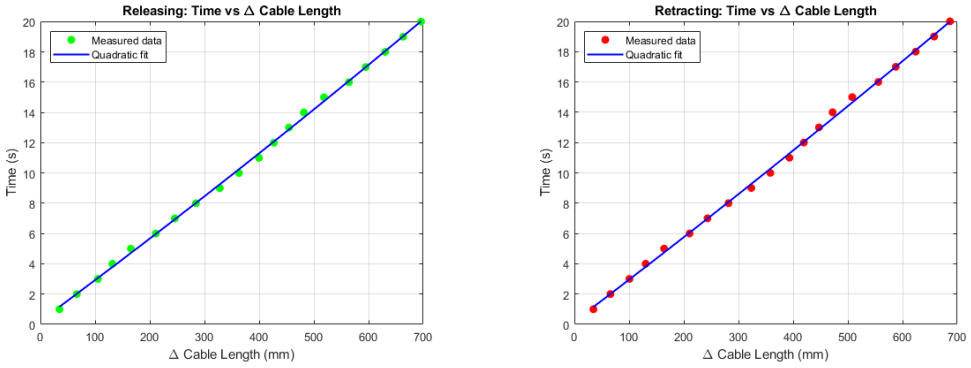

(a) Releasing direction (b) Retracting direction

Figure 3.8: Quadratic fitting of motor command time as a function of cable-length change.

During operation, the initial cable length is known. In this work, the initial cable length is 0.4 m. For a desired target cable length L_{tar}, the required commanded length change is calculated as

$$\Delta L_{\text{cmd}} = 1000 \left| L_{\text{tar}} - L_{\text{cur}} \right|, \tag{3.5}$$

where L_{cur} is the current known cable length in meters, L_{tar} is the desired target cable length in meters, and ΔL_{cmd} is expressed in millimeters. If $L_{\text{tar}} > L_{\text{cur}}$, the release relationship in Eq.(3.3) is used. If $L_{\text{tar}} < L_{\text{cur}}$, the retraction relationship in Eq.(3.4) is used.

After the motor command is applied, the cable length used by the system is updated to the commanded target value. Equivalently, for a release command,

$$L_{k+1} = L_k + \frac{\Delta L_{\text{cmd}}}{1000}, \tag{3.6}$$

and for a retraction command,

$$L_{k+1} = L_k - \frac{\Delta L_{\text{cmd}}}{1000}. \tag{3.7}$$

Here, L_k is the known cable length before the command, and L_{k+1} is the cable length after the command according to the commanded target. Since no direct cable-length feedback is used during operation, the difference between the commanded and achieved cable-length changes is quantified through validation experiments.

The fitted relationships were validated by commanding target cable-length changes of 100 mm, 200 mm, 300 mm, 400 mm, 500 mm, and 600 mm in both release and retraction directions. For each target value, the motor command time was computed using the corresponding fitted equation and applied to the motor. Each target command was repeated for several times, and the achieved cable-length change was measured using the OptiTrack system. The error for each validation trial was defined as

$$e_i = \Delta L_{\text{meas},i} - \Delta L_{\text{cmd}}, \tag{3.8}$$

where $\Delta L_{\text{meas},i}$ is the measured cable-length change for trial i, and ΔL_{cmd} is the commanded cable-length change. The validation performance was evaluated using the mean measured

cable-length change, mean absolute error, root-mean-square error, and maximum absolute error:

$$\mathrm{MAE} = \frac{1}{N}\sum_{i=1}^{N}|e_i|, \tag{3.9}$$

$$\mathrm{RMSE} = \sqrt{\frac{1}{N}\sum_{i=1}^{N}e_i^2}, \tag{3.10}$$

$$e_{\max} = \max_i |e_i|, \tag{3.11}$$

where N is the number of repeated trials for each target cable-length change.

Table 3.5 shows the validation results for the cable-release direction. The measured values are close to the commanded values across the tested range, with mean absolute errors between approximately 4.8 mm and 14.1 mm.

Table 3.6 shows the validation results for the cable-retraction direction. The calibrated relationship also provides practical retraction performance, although the error increases at the largest tested command value. This behavior is expected in an open-loop mechanism because cable winding, cable tension, spool layering, friction, and motor response can vary between trials.

Table 3.5: Validation results for cable release.

Commanded ΔL (mm)	Mean measured ΔL (mm)	MAE (mm)	RMSE (mm)	Max. error (mm)
100	107	7.2	7.5	10
200	204.2	4.8	5.9	9
300	313.3	14.1	17.1	25
400	404.9	11.3	14.2	32
500	504.4	5.0	6.6	11
600	608.7	13.1	13.9	22

Table 3.6: Validation results for cable retraction.

Commanded ΔL (mm)	Mean measured ΔL (mm)	MAE (mm)	RMSE (mm)	Max. error (mm)
100	105.1	5.1	5.2	7
200	198.4	4.2	4.6	7
300	308.7	10.5	12.6	18
400	402.0	9.2	16.9	31
500	508.2	13.2	14.6	25
600	621.1	21.1	21.6	27

These errors should be interpreted in relation to the intended function of the mechanism. In the present water-sampling experiments, the objective of cable adjustment is to lower the sampling payload sufficiently into the water and then retrieve it, rather than to regulate an exact sampling depth. The measured errors were therefore acceptable for the mission conditions investigated in this thesis. However, this result does not establish a universal allowable cable-length error. Applications requiring accurate payload depth, precise placement, or operation with small geometric clearances would require an application-specific accuracy requirement and may require direct cable-length feedback.

The calibration and validation results demonstrate that the command based method can provide practical cable-length adjustment without a direct cable-length sensor. The method is suitable for the mission structure considered in this work because cable adjustment is performed during payload lowering and retrieval phases, while the cable length is kept fixed during translational flight.

The developed mechanism provides the UAV slung payload system with the capability to release and retract the cable in a repeatable manner without using a direct cable-length sensor. With the cable-adjustment mechanism fabricated, integrated, and validated, the system is ready to support payload lowering and retrieval operations. The following chapter focuses on the swing-reduction technique used for the UAV suspended payload system during translational motion.

4 Input Shaping for Swing Reduction

This chapter presents the input shaping method used to reduce payload swing in the UAV suspended-payload system. It first introduces the dynamic representation of the quadrotor and suspended payload used to describe the coupled system behavior. A simplified payload swing model is then used to identify the dominant vibration mode required for shaper design. Based on this model, Zero Vibration (ZV) and Zero Vibration and Derivative (ZVD) input shapers are formulated and integrated into the UAV command architecture. The effectiveness of the proposed swing-reduction approach is then evaluated through simulation and experimental tests, with attention to vibration reduction, tracking behavior, and sensitivity to cable-length variation.

4.1 Quadrotor Suspended Payload Dynamics

The UAV suspended-payload system is modeled as a coupled quadrotor payload system in which the payload is attached to the vehicle through a cable of length L. The payload motion is described by two swing angles, θ_x and θ_y, which represent the payload deflection with respect to the vertical direction in the two lateral planes. This type of system is underactuated because the payload swing is not directly actuated, but is instead influenced by the motion of the quadrotor. Therefore, quadrotor translation and payload oscillation are dynamically coupled, and the payload swing must be considered when analyzing transportation motion.

Figure 4.1 illustrates the quadrotor suspended-payload configuration used in this work. The figure shows the quadrotor, the suspended payload, the cable length, and the payload swing angles used to describe the load motion.

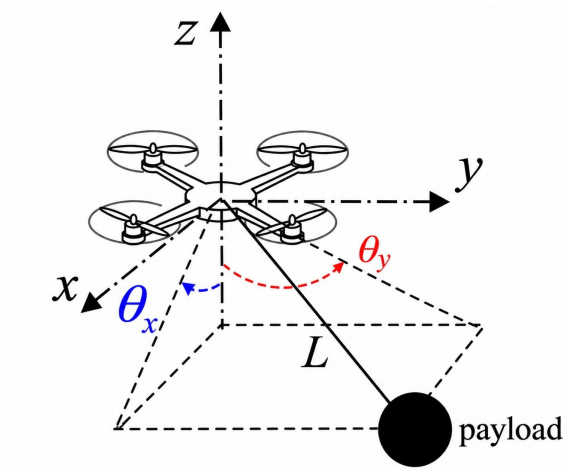

Figure 4.1: Schematic representation of the quadrotor suspended-payload system showing the cable length L and payload swing angles θ_x and θ_y.

Following [29], the outer-loop state vector of the suspended-payload system is written as

$$q = \begin{bmatrix} \xi^T & \theta_x & \theta_y \end{bmatrix}^T, \tag{4.1}$$

where

$$\xi = \begin{bmatrix} x & y & z \end{bmatrix}^T \tag{4.2}$$

is the quadrotor position in the inertial frame, and θ_x and θ_y are the payload swing angles. Using a Lagrangian formulation, the coupled translational and payload-swing dynamics can be expressed in compact form as

$$M_c(q)\ddot{q} + V_c(q,\dot{q})\dot{q} + G(q) = u, \tag{4.3}$$

where $M_c(q)$ is the inertia matrix, $V_c(q,\dot{q})\dot{q}$ represents the Coriolis and centrifugal terms, $G(q)$ is the gravitational term, and u is the generalized input vector associated with the quadrotor translational actuation. This model captures the coupling between quadrotor motion and payload swing and provides the dynamic basis used for the suspended-payload simulation model in this thesis.

In addition to the outer-loop motion, the quadrotor attitude dynamics determine the orientation required to generate the translational forces acting on the system. However, since the focus of this chapter is on payload swing reduction during transportation motion, the detailed attitude-control design is not repeated here. Instead, the compact model in Eq.(4.3) is used to represent the essential coupled behavior of the quadrotor and suspended payload.

For the analysis and evaluation in this thesis, several operating assumptions are adopted. Cable adjustment is not performed during translational UAV motion; instead, the cable length is treated as fixed during each transportation segment, while release and retraction are performed during hovering phases. The swing-reduction design therefore considers the dominant payload oscillation corresponding to a fixed cable configuration. Input shaping is applied only to the horizontal position-reference commands in the x and y directions, while the existing UAV position and attitude controllers remain unchanged. The payload motion is represented using the two swing angles θ_x and θ_y, and the dominant swing dynamics used for shaper parameterization are approximated by a second-order pendulum-like mode characterized by the natural frequency ω_n and damping ratio ζ.

The dynamic model in this subsection provides the basis for analyzing payload oscillation and evaluating the input shaping approach introduced in the following subsection.

4.2 Input Shaper Formulation and Parameterization

Input shaping is a feedforward command-design technique used to reduce residual vibration in oscillatory systems. The method was originally introduced as a command preshaping approach for flexible systems [13] and has since been widely used for vibration reduction in mechanical systems [14]. The main idea is to modify the reference command before it is applied to the system so that the vibration generated by one part of the command is cancelled by the vibration generated by later parts of the command. Therefore,

instead of changing the feedback controller, input shaping modifies the command signal sent to the system.

In this work, input shaping is applied to the UAV reference command in order to reduce the excitation of the suspended-payload swing. The shaped command is generated by convolving the original command with a sequence of impulses. If $r(t)$ is the original reference command, the shaped command $r_s(t)$ can be written as

$$r_s(t) = \sum_{i=1}^{n} A_i r(t - t_i), \tag{4.4}$$

where A_i is the amplitude of the i-th impulse, t_i is the time location of the i-th impulse, and n is the number of impulses in the input shaper. Each impulse produces a delayed and scaled version of the original command. The sum of these delayed commands forms the shaped reference command.

The impulse amplitudes are selected to satisfy the unity-gain condition,

$$\sum_{i=1}^{n} A_i = 1, \tag{4.5}$$

which ensures that the final value of the shaped command is equal to the final value of the original command. This condition is important because the input shaper should reduce vibration without changing the commanded final position.

As shown in Figure 4.2, input shaping can be interpreted as applying a sequence of time-delayed command components. When the impulse amplitudes and time locations are selected properly, the oscillatory response caused by one impulse is counteracted by the response caused by the following impulses. This cancellation reduces the residual vibration after the command is completed.

The shaper design is based on the dominant vibration mode of the suspended payload. This vibration mode can be represented using a standard second-order model,

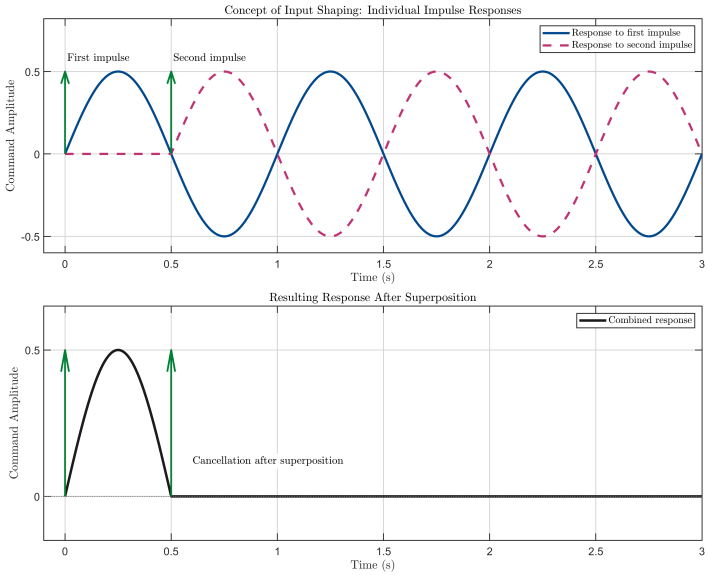

Figure 4.2: Input shaping concept.

$$G(s) = \frac{\omega_n^2}{s^2 + 2\zeta\omega_n s + \omega_n^2}, \tag{4.6}$$

where ω_n is the natural frequency and ζ is the damping ratio. The corresponding damped natural frequency is

$$\omega_d = \omega_n \sqrt{1-\zeta^2}. \tag{4.7}$$

For a suspended payload, the dominant swing frequency is mainly influenced by the cable length. A nominal estimate of the natural frequency can be obtained from the pendulum approximation,

$$\omega_n \approx \sqrt{\frac{g}{L}}, \tag{4.8}$$

where g is the gravitational acceleration and L is the cable length. In practice, the shaper can also be tuned using experimentally identified values of ω_n and ζ, which provides a

more accurate representation of the actual payload swing response.

For a sequence of impulses, the residual vibration depends on the impulse amplitudes and their time locations. The vibration response can be separated into cosine and sine components [13], written as

$$C(\omega_n, \zeta) = \sum_{i=1}^{n} A_i e^{-\zeta \omega_n t_i} \cos(\omega_d t_i), \tag{4.9}$$

$$S(\omega_n, \zeta) = \sum_{i=1}^{n} A_i e^{-\zeta \omega_n t_i} \sin(\omega_d t_i). \tag{4.10}$$

The residual vibration magnitude after the impulse sequence is proportional to

$$V(\omega_n, \zeta) = e^{-\zeta \omega_n t_n} \sqrt{C^2(\omega_n, \zeta) + S^2(\omega_n, \zeta)}. \tag{4.11}$$

Therefore, the input shaper design problem is to select A_i and t_i so that the residual vibration is reduced or cancelled for the selected vibration parameters.

For zero residual vibration, the cosine and sine components of the residual vibration must both be equal to zero. Therefore, the zero-vibration constraints are written as

$$C(\omega_n, \zeta) = 0, \tag{4.12}$$

$$S(\omega_n, \zeta) = 0. \tag{4.13}$$

In addition, the first impulse is applied at the beginning of the command,

$$t_1 = 0, \tag{4.14}$$

and the impulse amplitudes satisfy

$$\sum_{i=1}^{n} A_i = 1, \qquad A_i > 0. \tag{4.15}$$

The unity-gain condition preserves the final command value, while the positive-amplitude condition avoids reversing the direction of the command. These constraints form the basis for the Zero Vibration shaper.

For the Zero Vibration (ZV) shaper, two impulses are used. Setting $n = 2$, $t_1 = 0$, and choosing the smallest positive impulse spacing gives

$$t_2 = T_d = \frac{\pi}{\omega_d}. \tag{4.16}$$

The shaper parameters are expressed using

$$K = \exp\left(\frac{-\zeta\pi}{\sqrt{1-\zeta^2}}\right), \tag{4.17}$$

and

$$T_d = \frac{\pi}{\omega_d}. \tag{4.18}$$

Solving the zero-vibration constraints with the unity-gain condition gives the ZV impulse amplitudes as

$$A_1 = \frac{1}{1+K}, \qquad A_2 = \frac{K}{1+K}. \tag{4.19}$$

Therefore, the ZV impulse sequence is

$$\begin{bmatrix} A_i \\ t_i \end{bmatrix}_{\text{ZV}} = \begin{bmatrix} \frac{1}{1+K} & \frac{K}{1+K} \\ 0 & T_d \end{bmatrix}. \tag{4.20}$$

The ZV shaper cancels residual vibration for the selected values of ω_n and ζ. Since it uses only two impulses, it has a short duration and introduces less delay into the command. However, its performance depends on the accuracy of the assumed vibration parameters. If the actual natural frequency differs from the design value, residual swing can remain after the motion.

To improve robustness to modeling errors, the Zero Vibration and Derivative (ZVD) shaper adds derivative constraints to the zero-vibration constraints. These derivative constraints reduce the sensitivity of residual vibration to errors in the assumed natural frequency. The additional constraints are written as

$$\frac{\partial C(\omega_n, \zeta)}{\partial \omega_n} = 0, \tag{4.21}$$

$$\frac{\partial S(\omega_n, \zeta)}{\partial \omega_n} = 0. \tag{4.22}$$

Equivalently, these constraints can be represented in terms of the impulse sequence as

$$\sum_{i=1}^{n} A_i t_i e^{-\zeta \omega_n t_i} \sin(\omega_d t_i) = 0, \tag{4.23}$$

$$\sum_{i=1}^{n} A_i t_i e^{-\zeta \omega_n t_i} \cos(\omega_d t_i) = 0. \tag{4.24}$$

The derivative constraints make the residual vibration curve flatter near the design frequency. As a result, small errors in the estimated natural frequency have less effect on the vibration-reduction performance. To satisfy these additional constraints, the ZVD shaper uses three impulses located at 0, T_d, and $2T_d$.

Solving the ZV constraints together with the derivative constraints gives the ZVD impulse sequence as

$$\begin{bmatrix} A_i \\ t_i \end{bmatrix}_{\text{ZVD}} = \begin{bmatrix} \frac{1}{(1+K)^2} & \frac{2K}{(1+K)^2} & \frac{K^2}{(1+K)^2} \\ 0 & T_d & 2T_d \end{bmatrix}. \tag{4.25}$$

Figure 4.3 compares the sensitivity of the ZV and ZVD shapers to errors in the assumed natural frequency. The horizontal axis represents the ratio between the actual vibration frequency and the design frequency, while the vertical axis represents the residual vibration amplitude. The ZV shaper produces a sharp reduction in residual vibration near the design frequency, but its performance degrades quickly when the frequency ratio moves away from unity. In contrast, the ZVD shaper has a wider low vibration region, which indicates improved robustness to natural-frequency mismatch. This behavior is expected because the ZVD shaper satisfies additional derivative constraints on the residual vibration.

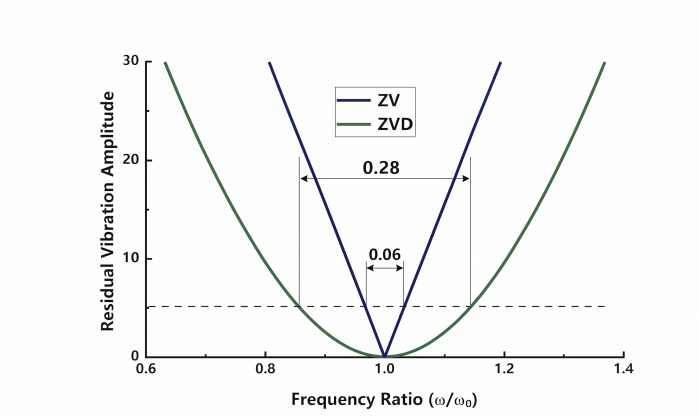

Figure 4.3: Sensitivity curves of ZV and ZVD input shapers [14].

Compared with the ZV shaper, the ZVD shaper increases the command duration because of the additional impulse. However, it provides improved robustness when the actual payload swing frequency differs from the design value. This tradeoff is important in suspended payload systems because the swing response can be affected by cable length, payload configuration, and experimental conditions.

An important limitation of the feedforward input-shaping approach is that it is primar-

ily designed to reduce vibration excited by the commanded UAV motion. An unmeasured external disturbance can excite the suspended payload independently of the shaped reference command. Since the present implementation does not use payload-swing feedback, the input shaper cannot directly compensate for such disturbance-induced oscillations. The UAV feedback controller may reject part of the disturbance acting on the vehicle, but additional payload swing can remain. Consequently, the results presented in this thesis demonstrate command-induced swing reduction under the tested indoor conditions and do not establish disturbance-rejection performance.

In this thesis, both ZV and ZVD shapers are evaluated for suspended payload swing reduction. The shaper parameters are calculated using the selected values of ω_n and ζ, and the resulting shaped commands are applied to the UAV reference command before position tracking. The implementation of these shaped commands in the UAV control architecture is described in the following subsection.

4.3 Implementation in the UAV Command Architecture

The input shaper is implemented in the reference command channel before the UAV position control system. The purpose of this placement is to modify the commanded motion before it is tracked by the controller, while keeping the feedback control structure unchanged. Therefore, the input shaper acts as a feedforward command filter that reshapes the reference command to reduce the excitation of the suspended-payload swing.

The command architecture used for input shaping is shown in Figure. 4.4. The original reference command is first generated for the desired UAV motion. This command is then passed through the selected input shaper. Three cases are considered for comparison: the unshaped command, the ZV shaped command, and the ZVD shaped command. The resulting reference command is then sent to the position control system, which drives the quadrotor suspended-payload system.

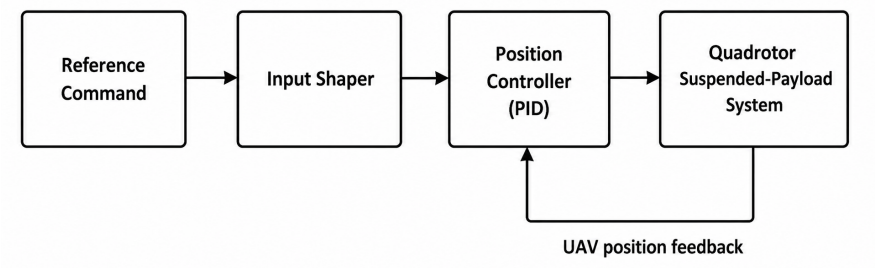

Figure 4.4: Implementation of the input shaper in the UAV command architecture.

In this work, the input shaper is applied to the position reference command in two translational directions (x,y). The reference command vector to be shaped is defined as

$$\mathbf{r}(t) = \begin{bmatrix} x_d(t) & y_d(t) \end{bmatrix}^T, \tag{4.26}$$

where $x_d(t)$, and $y_d(t)$ are the desired position commands in the inertial frame. The shaped reference command is obtained by applying the impulse sequence to the reference vector as

$$\mathbf{r}_s(t) = \sum_{i=1}^{n} A_i \mathbf{r}(t - t_i), \tag{4.27}$$

where $\mathbf{r}_s(t)$ is the shaped reference command, A_i is the impulse amplitude, t_i is the impulse time location, and n is the number of impulses. This vector form shows that the same input shaping operation is applied to the commanded x, and y position references.

For the unshaped case, the reference command is applied directly to the position-control system,

$$\mathbf{r}_{\text{un}}(t) = \mathbf{r}(t). \tag{4.28}$$

For the ZV shaped case, the reference command is formed using two delayed command components,

$$\mathbf{r}_{\mathrm{ZV}}(t) = A_1\mathbf{r}(t) + A_2\mathbf{r}(t - T_d). \tag{4.29}$$

For the ZVD shaped case, the reference command is formed using three delayed command components,

$$\mathbf{r}_{\mathrm{ZVD}}(t) = A_1\mathbf{r}(t) + A_2\mathbf{r}(t - T_d) + A_3\mathbf{r}(t - 2T_d). \tag{4.30}$$

The shaped commands preserve the final commanded position because the impulse amplitudes satisfy the unity-gain condition. As a result, the UAV is commanded to reach the same final position in the unshaped, ZV shaped, and ZVD shaped cases, while the time profile of the command is modified to reduce payload excitation.

Although payload swing is mainly excited by the acceleration of the UAV support point, the implemented command structure uses position references. Applying the input shaper to the position reference also shapes the corresponding velocity and acceleration profiles because the shaped command is a linear combination of delayed reference commands. Therefore, the acceleration profile that excites the payload swing is indirectly modified without requiring direct acceleration command control.

This implementation allows the input shaper to be integrated without changing the position controller or the inner-loop UAV control structure. The same reference command can therefore be used to compare the unshaped, ZV shaped, and ZVD shaped responses. The resulting UAV motion and payload swing are then evaluated using the performance metrics described in the simulation and experimental evaluation subsections.

4.4 Simulation Evaluation

This subsection evaluates the effectiveness of input shaping for reducing suspended-payload swing in simulation. Three command cases are compared: an unshaped reference

command, a Zero Vibration (ZV) shaped command, and a Zero Vibration and Derivative (ZVD) shaped command. The same suspended-payload model and position-control structure are used in all cases so that differences in the payload response can be attributed to the command-shaping method.

The simulation evaluation is organized into three studies. The first study evaluates the nominal input shaping response under the design cable length and nominal payload mass. The second study evaluates the sensitivity of the shapers to cable-length mismatch by changing the actual cable length while keeping the shaper design fixed. The third study examines the effect of payload-mass variation on the swing response. These simulation studies are summarized in Table 4.1.

Table 4.1: Simulation studies used to evaluate the input shaping method.

Study	Purpose	Compared cases
Nominal input shaping	Evaluate swing reduction.	Unshaped, ZV, ZVD
Cable-length mismatch	Evaluate sensitivity to cable-length variation.	Unshaped, ZV, ZVD
Payload-mass variation	Evaluate sensitivity to payload-mass variation.	Unshaped, ZV, ZVD

4.4.1 Simulation Setup and Evaluation Metrics

The nominal simulation parameters are listed in Table 4.2. The design natural frequency is calculated using the pendulum approximation introduced in Eq.(4.8). For the nominal design case, $L = 1$ m, which gives $\omega_n = 3.13$ rad/s. The UAV is initialized with zero payload swing and zero initial motion.

The simulation results in this section correspond to the modeled UAV suspended-payload system under the parameters listed in Table 4.2. The UAV begins with zero initial payload swing and zero initial motion. The cable length remains fixed during each simulated maneuver, and no cable release or retraction is performed while the UAV is translating. The same UAV control structure and reference motion are used for the unshaped, ZV-shaped, and ZVD-shaped comparisons; only the reference command

Table 4.2: Nominal simulation parameters for the input shaping evaluation.

Parameter	Symbol	Value
UAV mass	m_q	1.6 kg
Payload mass	m_p	0.2 kg
Cable length	L	1 m
Gravitational acceleration	g	9.81 m/s^2
Design natural frequency	ω_n	3.13 rad/s
Damping ratio	ζ	0.063
Reference command in x	x_d	2 m
Reference command in y	y_d	3 m
Altitude command	z_d	1.5 m
Simulation duration	T_s	15 s

provided to the position controller is changed. The simulation studies therefore isolate the effect of input shaping under the considered model and parameter variations.

For the nominal simulation case, the damping ratio is set to $\zeta = 0.063$, representing the actual physical system. Using $L = 1$ m, the design natural frequency is $\omega_n = 3.1321$ rad/s. The corresponding damped natural frequency and impulse spacing are calculated as

$$\omega_d = \omega_n \sqrt{1-\zeta^2} = 3.1259 \text{ rad/s}, \tag{4.31}$$

$$T_d = \frac{\pi}{\omega_d} = 1.0050 \text{ s}. \tag{4.32}$$

The resulting ZV and ZVD impulse sequences are listed in Table 4.3. The impulse amplitudes are calculated from the shaper coefficient K using the input shaper design equations presented earlier in this chapter.

Table 4.3: Input shaper parameters used in the nominal simulation case.

Shaper	Impulse amplitudes A_i	Impulse times t_i (s)
ZV	[0.5494, 0.4506]	[0, 1.0050]
ZVD	[0.3019, 0.4951, 0.2030]	[0, 1.0050, 2.0101]

The payload response is evaluated using four swing-angle metrics: maximum absolute swing angle, peak-to-peak swing angle, root-mean-square value, and mean absolute error.

These metrics are computed separately for θ_x and θ_y. For a swing response $\theta(t)$, the maximum absolute swing angle is defined as

$$\theta_{\max} = \max_t |\theta(t)|, \tag{4.33}$$

the peak-to-peak swing angle is defined as

$$\theta_{\text{p2p}} = \max_t \theta(t) - \min_t \theta(t), \tag{4.34}$$

the RMS value is defined as

$$\theta_{\text{RMS}} = \sqrt{\frac{1}{N}\sum_{k=1}^{N} \theta^2(k)}, \tag{4.35}$$

and the mean absolute error is defined as

$$\theta_{\text{MAE}} = \frac{1}{N}\sum_{k=1}^{N} |\theta(k)|. \tag{4.36}$$

The maximum and peak-to-peak values quantify the largest swing excursions, while the RMS and MAE values describe the overall oscillatory content over the simulation interval.

4.4.2 Nominal Input Shaping Evaluation

The nominal simulation case compares the unshaped, ZV shaped, and ZVD shaped commands using the parameters listed in Table 4.2. Figure 4.5 shows the reference commands in the x and y directions. The shaped commands reach the same final values as the unshaped command, confirming that the unity-gain condition preserves the desired final position. However, the shaped commands distribute the command over delayed impulses. As a result, the ZV command reaches the final value later than the unshaped

command, while the ZVD command introduces the longest command duration because it contains an additional impulse.

The unshaped, ZV-shaped, and ZVD-shaped cases do not have identical command durations. This difference is inherent to input shaping: the ZV shaper introduces a delay of approximately T_d, while the ZVD shaper introduces a delay of approximately $2T_d$ because of the additional delayed impulse. Therefore, the comparison in this thesis should be interpreted as an evaluation of the tradeoff between vibration reduction and increased maneuver duration, rather than as a comparison under identical transition times. All cases use the same initial and final positions and the same underlying UAV controller, while only the reference-command profile is modified by the input shaper.

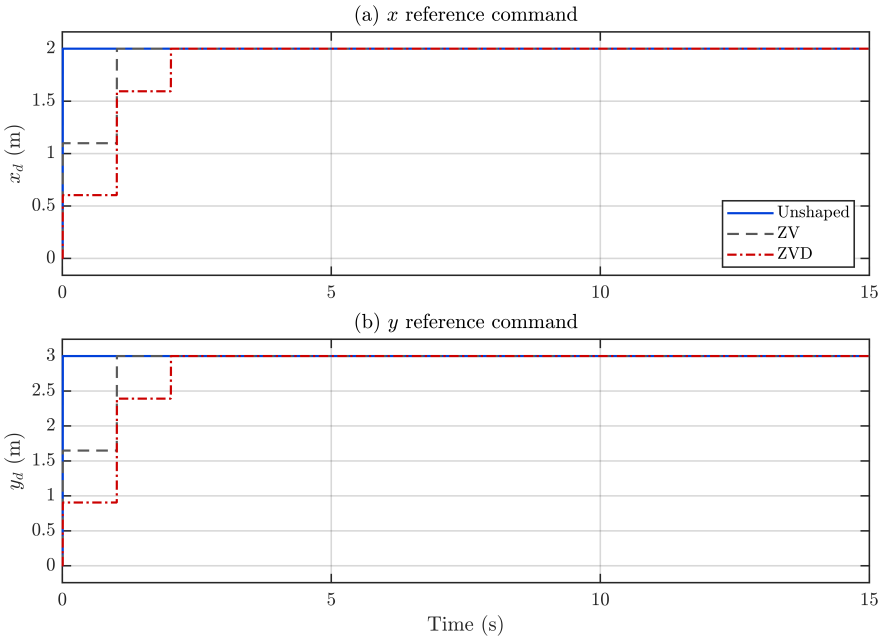

Figure 4.5: Reference commands for the nominal simulation case.

The UAV position responses are shown in Figure 4.6. All three cases converge to the desired final position. The unshaped command produces the fastest position change, while the shaped commands produce smoother responses due to the delayed command components. This behavior is expected because input shaping modifies the command

timing before it is applied to the position controller.

Figures 4.7 and 4.8 show the payload swing responses in the x and y directions, respectively. The unshaped command produces the largest payload oscillations because the commanded motion excites the suspended-load mode. Both input shaped commands reduce the swing response compared with the unshaped command. The ZVD shaper gives the smallest swing amplitude in both directions, while the ZV shaper provides significant swing reduction with a shorter command delay.

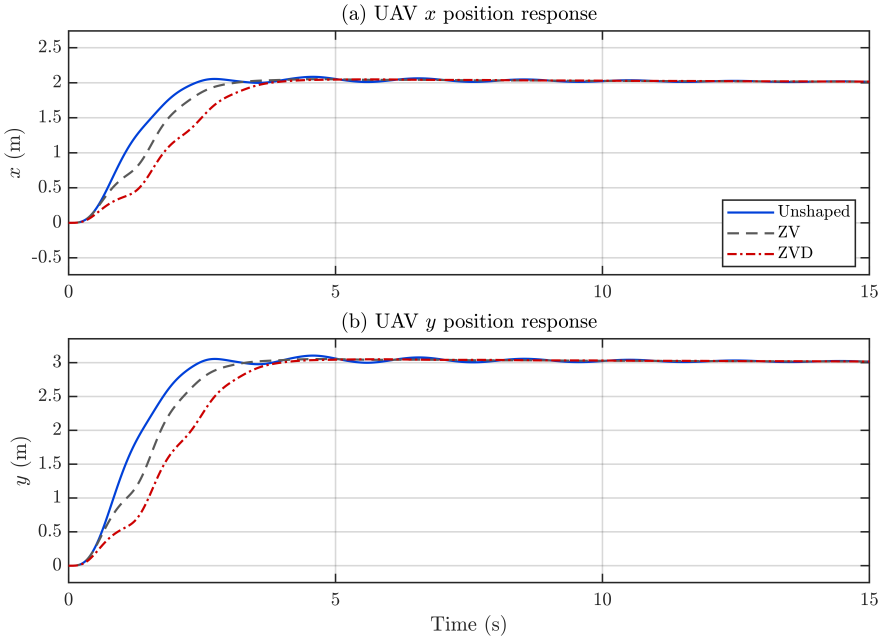

Figure 4.6: UAV position responses for the nominal simulation case.

The quantitative swing-angle results for the nominal case are summarized in Table 4.4. For θ_x, the ZV shaper reduces the maximum absolute swing angle from 43.22° to 18.47°, corresponding to a 57.3% reduction. The ZVD shaper further reduces the maximum absolute swing angle to 10.16°, corresponding to a 76.5% reduction. For θ_y, the ZV shaper reduces the maximum absolute swing angle from 45.01° to 25.13°, corresponding to a 44.2% reduction, while the ZVD shaper reduces it to 14.78°, corresponding to a 67.2% reduction. The RMS and MAE values show the same trend, indicating that the

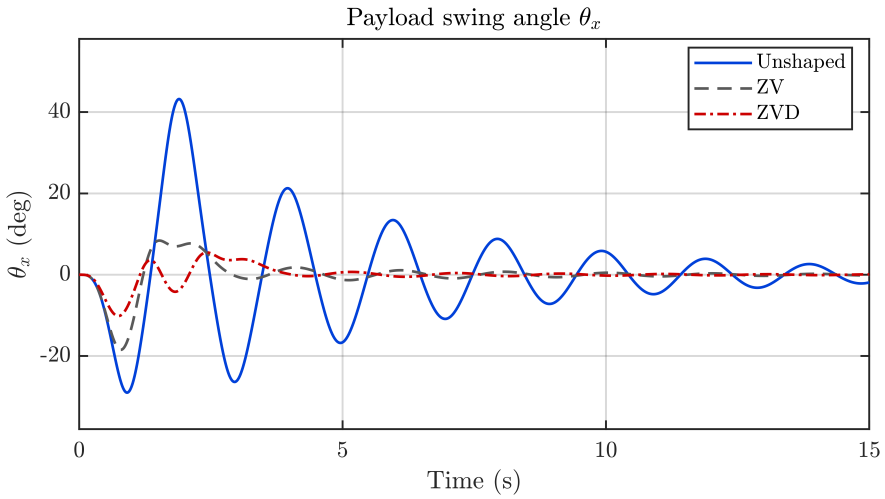

Figure 4.7: Payload swing response θ_x for the nominal simulation case.

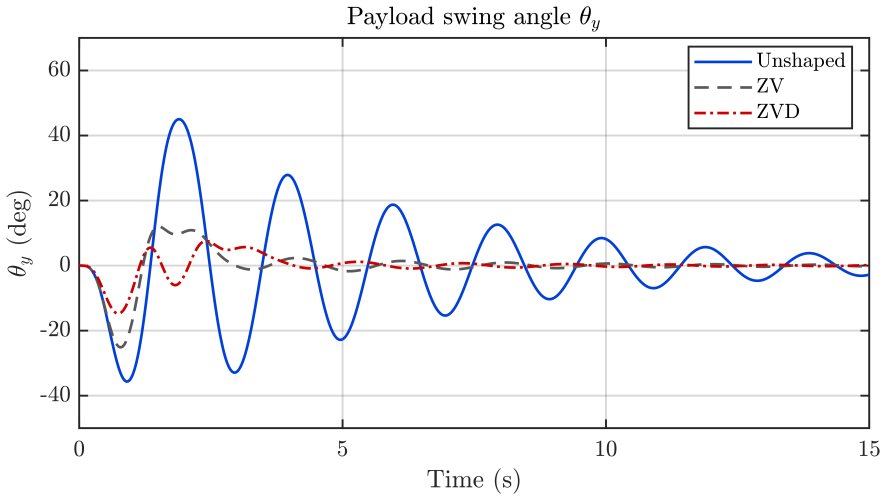

Figure 4.8: Payload swing response θ_y for the nominal simulation case.

input shapers reduce not only the peak swing amplitude but also the overall oscillatory content. Overall, the ZVD shaper provides the strongest swing attenuation in the nominal simulation case.

Table 4.4: Simulation swing-angle metrics for the reference command.

Case	Max. $\lvert\theta_x\rvert$ (deg)	P–P θ_x (deg)	RMS θ_x (deg)	MAE θ_x (deg)	Max. $\lvert\theta_y\rvert$ (deg)	P–P θ_y (deg)	RMS θ_y (deg)	MAE θ_y (deg)
unshaped	43.22	72.22	13.52	9.15	45.01	80.66	16.81	12.01
ZV	18.47	26.87	5.30	3.06	25.13	37.12	7.41	4.29
ZVD	10.16	15.64	3.11	1.90	14.78	22.35	4.54	2.82

4.4.3 Cable-Length Mismatch Evaluation

The cable-length mismatch study evaluates the sensitivity of the input shapers to errors in the assumed payload natural frequency. In this study, the ZV and ZVD shapers are designed using the nominal cable length $L_d = 1$ m, while the actual simulated cable length is changed to $L_a = 0.8$ m and $L_a = 1.2$ m. All other simulation settings and controller parameters are retained from the nominal case. Therefore, the mismatch study changes the actual cable length while keeping the input-shaper design fixed, allowing the effect of natural-frequency mismatch to be examined separately from changes in the shaper parameters.

The mismatch cases are summarized in Table 4.5. A shorter cable increases the actual natural frequency, while a longer cable decreases it. Therefore, the 0.8 m and 1.2 m cases evaluate the shaper response when the actual system is faster and slower than the nominal design model, respectively.

Table 4.5: Cable-length mismatch cases used in simulation.

Case	Design length L_d	Actual length L_a	$\omega_{n,a}$	Frequency ratio
Nominal	1.0 m	1.0 m	3.13 rad/s	1.00
Shorter cable	1.0 m	0.8 m	3.50 rad/s	1.12
Longer cable	1.0 m	1.2 m	2.86 rad/s	0.91

Figures 4.9 and 4.10 show the swing responses for the shorter-cable mismatch case, where the actual cable length is 0.8 m. The unshaped command produces large oscillations in both swing directions. Both input shapers reduce the swing response, with the ZVD shaper producing the lowest oscillation amplitude.

Figures 4.11 and 4.12 show the corresponding swing responses for the longer-cable mismatch case, where the actual cable length is 1.2 m. Similar to the shorter-cable case, the shaped commands reduce the payload oscillation compared with the unshaped command. The ZVD shaper again produces the smallest swing response, indicating better

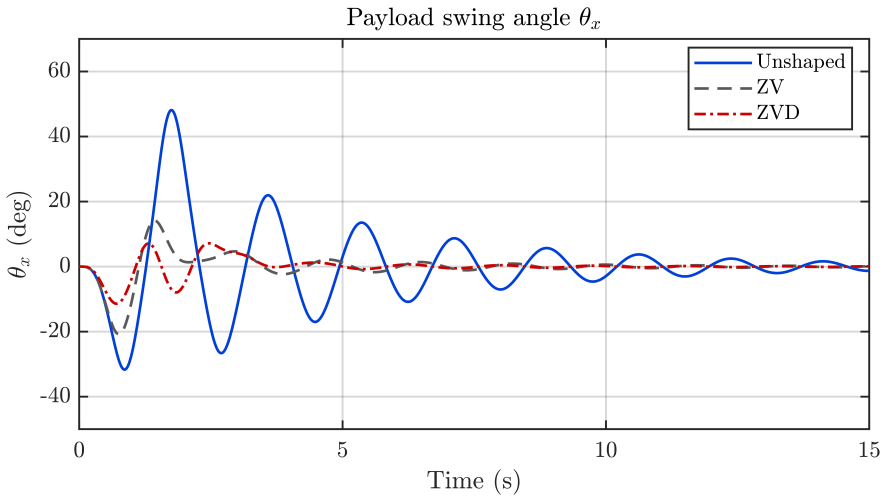

Figure 4.9: Payload swing response θ_x for the cable-length mismatch case $L_a = 0.8$ m.

tolerance to the natural-frequency mismatch considered in this simulation.

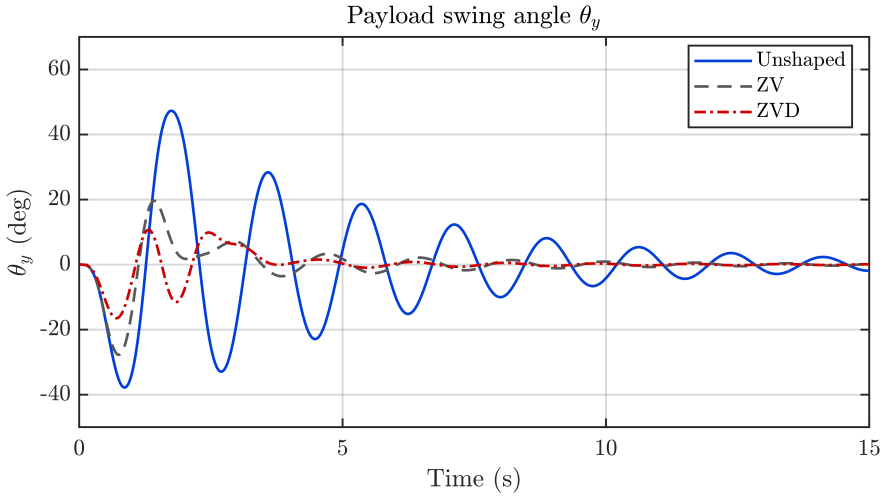

Figure 4.10: Payload swing response θ_y for the cable-length mismatch case $L_a = 0.8$ m.

The swing-angle metrics for the mismatch cases are summarized in Table 4.6. For the $L_a = 0.8$ m case, the ZVD shaper reduces the maximum absolute swing angle by 76.3% in θ_x and 65.1% in θ_y, while the ZV shaper reduces the corresponding values by 56.8% and 41.3%. For the $L_a = 1.2$ m case, the ZVD shaper reduces the maximum absolute swing angle by 76.8% in θ_x and 68.8% in θ_y, while the ZV shaper reduces the corresponding values by 57.8% and 46.6%. The RMS and MAE values show the same overall trend,

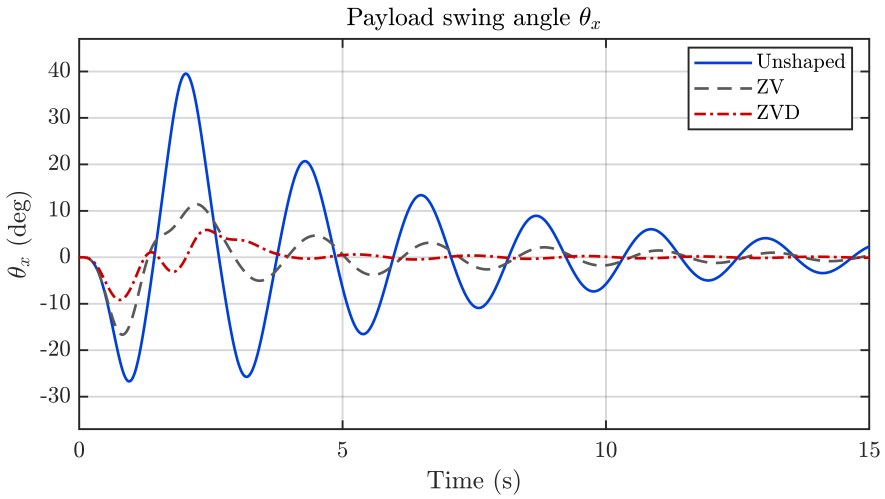

Figure 4.11: Payload swing response θ_x for the cable-length mismatch case $L_a = 1.2$ m.

with ZVD producing the lowest oscillatory content in both mismatch cases.

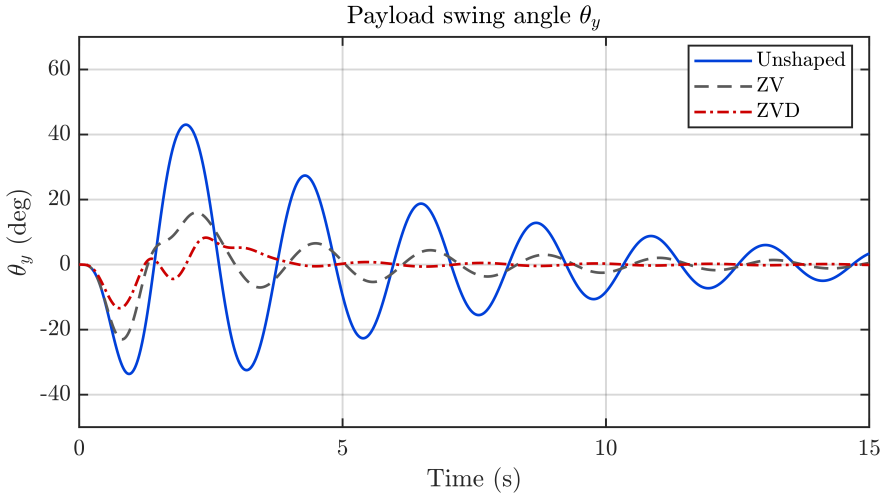

Figure 4.12: Payload swing response θ_y for the cable-length mismatch case $L_a = 1.2$ m.

Table 4.6: Swing-angle metrics for the cable-length mismatch cases.

Actual length	Case	Max. $\lvert\theta_x\rvert$ (deg)	P–P θ_x (deg)	RMS θ_x (deg)	MAE θ_x (deg)	Max. $\lvert\theta_y\rvert$ (deg)	P–P θ_y (deg)	RMS θ_y (deg)	MAE θ_y (deg)
0.8 m	Unshaped	48.11	79.79	13.75	8.71	47.29	85.09	16.54	11.19
0.8 m	ZV	20.79	34.91	5.53	3.13	27.74	47.34	7.69	4.45
0.8 m	ZVD	11.42	18.57	3.68	2.25	16.49	27.16	5.34	3.26
1.2 m	Unshaped	39.52	66.22	13.05	9.20	43.02	76.65	16.65	12.29
1.2 m	ZV	16.66	28.10	5.85	3.96	22.98	39.01	8.22	5.59
1.2 m	ZVD	9.18	15.06	3.00	1.78	13.41	21.69	4.35	2.58

These results show that the input shapers remain effective when the actual cable length differs from the nominal design value. The ZV shaper reduces the swing response in both mismatch cases, but the ZVD shaper provides lower maximum swing and lower RMS values for both $L_a = 0.8$ m and $L_a = 1.2$ m. This behavior is consistent with the wider low-vibration region of the ZVD shaper. At the same time, the mismatch study shows that the swing response depends on the relationship between the design frequency and the actual payload frequency, which supports the need to account for cable length when selecting the shaper parameters.

4.4.4 Payload-Mass Variation Evaluation

The payload-mass variation study evaluates the sensitivity of the input shaped response to changes in the transported payload mass. This study is relevant to suspended-payload transportation applications, where the UAV may carry payloads with different masses. The cable length and shaper design parameters are kept fixed, while the payload mass is varied from 0.1 kg to 0.5 kg. Unlike cable-length variation, changing the payload mass does not change the natural frequency predicted by the simple pendulum approximation. However, it changes the coupled UAV–payload dynamics and the effect of the suspended load on the UAV motion. Therefore, this study evaluates whether the swing reduction benefit of input shaping is maintained under changes in payload mass.

The payload-mass variation cases are summarized in Table 4.7. For all cases, the cable length is kept fixed at $L = 1$ m, and the ZV and ZVD shapers are designed using the same nominal cable length.

The swing-angle metrics for the payload-mass variation cases are summarized in Table 4.8. To keep the comparison focused, the table reports the maximum absolute swing angle and RMS swing angle for both θ_x and θ_y. These metrics are used to evaluate how the peak swing response and overall oscillatory content change as the payload mass is

Table 4.7: Payload-mass variation cases used in simulation.

Case	Payload mass m_p	Cable length L
Case 1	0.1 kg	1.0 m
Case 2	0.2 kg	1.0 m
Case 3	0.3 kg	1.0 m
Case 4	0.4 kg	1.0 m
Case 5	0.5 kg	1.0 m

varied while the cable length and shaper design are kept fixed.

To visualize the effect of payload-mass variation, the maximum swing angle and RMS swing angle are plotted for both θ_x and θ_y. Figure 4.13 shows the effect of payload mass on the maximum swing angle, while Figure 4.14 shows the corresponding effect on the RMS swing angle.

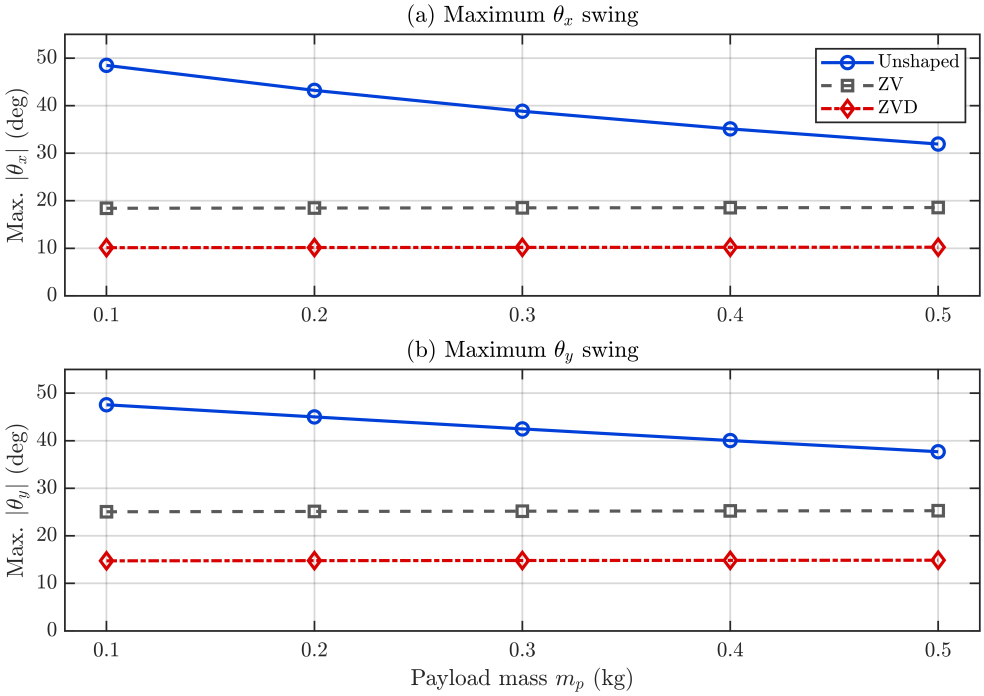

Figure 4.13: Effect of payload-mass variation on the maximum swing angle.

The payload-mass variation results show that both ZV and ZVD shaping reduce the maximum and RMS swing angles across all tested payload masses, from 0.1 kg to 0.5 kg. Although the unshaped swing decreases as the payload mass increases, this trend is

Table 4.8: Swing-angle metrics for the payload-mass variation cases.

Payload mass	Case	Max. $\lvert\theta_x\rvert$ (deg)	RMS θ_x (deg)	Max. $\lvert\theta_y\rvert$ (deg)	RMS θ_y (deg)
0.1 kg	Unshaped	48.48	16.46	47.57	20.30
0.1 kg	ZV	18.42	5.68	25.06	7.90
0.1 kg	ZVD	10.13	2.96	14.74	4.32
0.2 kg	Unshaped	43.22	13.52	45.01	16.81
0.2 kg	ZV	18.47	5.30	25.13	7.41
0.2 kg	ZVD	10.16	3.11	14.78	4.54
0.3 kg	Unshaped	38.83	11.86	42.49	14.91
0.3 kg	ZV	18.51	5.14	25.18	7.21
0.3 kg	ZVD	10.19	3.17	14.81	4.62
0.4 kg	Unshaped	35.12	10.97	40.04	13.95
0.4 kg	ZV	18.54	5.08	25.24	7.14
0.4 kg	ZVD	10.21	3.15	14.84	4.58
0.5 kg	Unshaped	31.93	10.25	37.69	13.18
0.5 kg	ZV	18.57	4.90	25.28	6.89
0.5 kg	ZVD	10.23	3.18	14.87	4.63

attributed to changes in the coupled closed-loop UAV–payload response under the same controller and reference command, rather than to a change in the swing frequency.

Overall, the results indicate that input shaping remains effective under payload-mass variation, with the ZVD shaper providing the strongest attenuation among all of the cases.

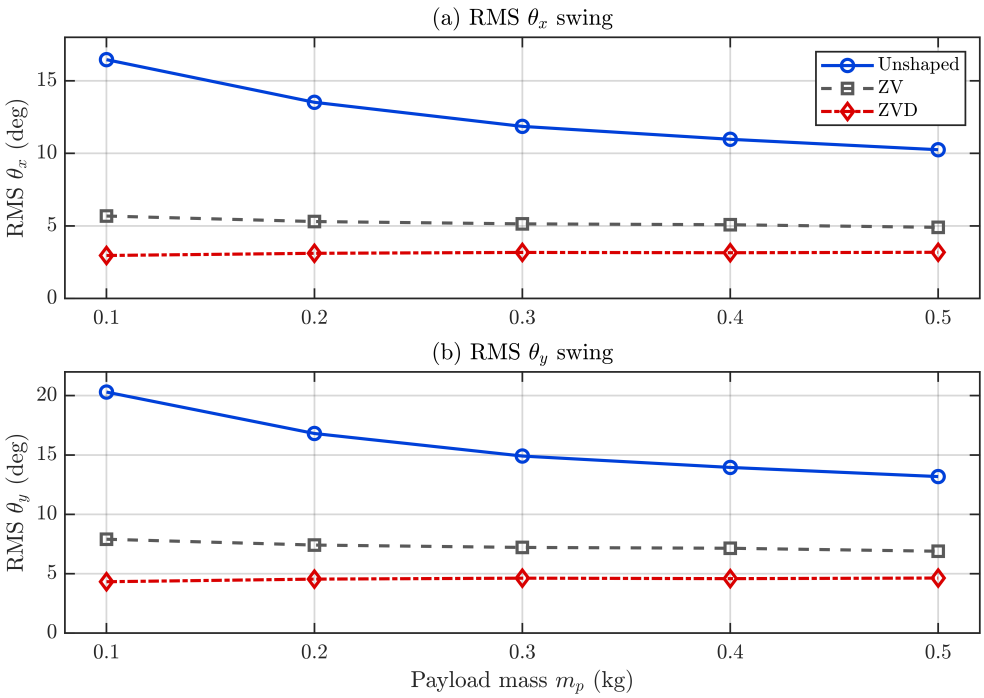

Figure 4.14: Effect of payload-mass variation on the RMS swing angle.

4.4.5 Summary of Simulation Results

The simulation results show that input shaping reduces suspended-payload swing compared with the unshaped reference command. In the nominal case, both ZV and ZVD input shapers reduce the maximum swing angle, peak-to-peak swing, RMS value, and MAE in both swing directions. The ZVD shaper provides the strongest swing attenuation, while the ZV shaper provides swing reduction with a shorter command duration.

The cable-length mismatch study shows that the input shapers remain effective when the actual cable length differs from the nominal design length. However, the results also show that the swing response depends on the relationship between the shaper design frequency and the actual payload natural frequency. This confirms the importance of accounting for cable length when selecting the shaper parameters. Across the tested mismatch cases, the ZVD shaper gives lower maximum swing and RMS values than the ZV shaper, which is consistent with its improved robustness to frequency variation.

The payload-mass variation study shows that the swing-reduction benefit is maintained over the tested payload-mass range. Although changing the payload mass does not change the natural frequency predicted by the simple pendulum approximation, it changes the coupled UAV–payload dynamics and the effect of the suspended load on the UAV motion. The shaped responses remain consistently lower than the unshaped response for all tested payload masses, with the ZVD shaper producing the lowest swing levels.

Overall, the simulation results support the use of input shaping as a feedforward swing-reduction method for the cable-suspended UAV system. The results also show the tradeoff between the shorter duration of the ZV shaper and the improved attenuation and robustness of the ZVD shaper. The following subsection evaluates the input shaping method experimentally using the UAV suspended-payload test platform.

4.5 Experimental Evaluation

This subsection presents the hardware test used to evaluate the input shaping method on the UAV suspended-payload platform. The purpose of the experiment is to verify that the swing-reduction behavior observed in simulation is also achieved during real flight. The hardware test compares three command cases: the unshaped command, the ZV shaped command, and the ZVD shaped command. The comparison focuses on the y-direction motion because the test maneuver is performed from an initial point to a final point along the y-axis while keeping the x position and altitude fixed.

4.5.1 Experimental Setup

Hardware experiments are conducted to verify the effectiveness of input shaping using the experimental setup shown in Fig. 4.15. The experimental system consists of a Quanser QDrone2 quadrotor, an OptiTrack motion-capture system with 16 Flex 13 cameras, a workstation, and a router. The Ground Station calculates the pose of the quadrotor and

payload using Motive, the software provided with the OptiTrack system, at 100 Hz [61]. The QDrone2 is equipped with four brushless motors, an NVIDIA Jetson Xavier NX compute board, a 1 kHz IMU sensor, multiple high-resolution cameras, and built-in Wi-Fi [59]. Figure 4.15 also shows the information flow during the experiment.

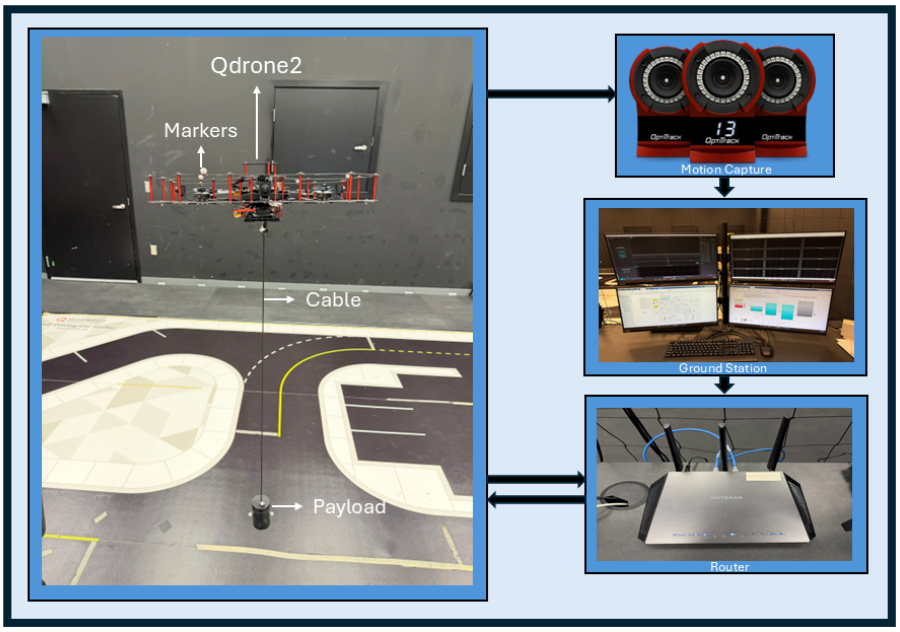

Figure 4.15: Experimental setup for the UAV suspended-payload input shaping test.

The hardware test parameters are summarized in Table 4.9. The cable length is fixed at $L = 1.0$ m, and the payload mass is 0.2 kg. The UAV is commanded to move from the initial position $(0, -1.5, 1.5)$ to the final position $(0, 1.5, 1.5)$, while the x-position and altitude are kept fixed. The input shapers are designed using payload swing parameters identified from flight data, with $\omega_n = 3.2$ rad/s and $\zeta = 0.063$.

Table 4.9: Experimental hardware test parameters.

Parameter	Symbol	Value
UAV mass	m_q	1.6 kg
Payload mass	m_p	0.2 kg
Cable length	L	1.0 m
Initial position	$\mathbf{p}_0$	$(0,-1.5,1.5)$ m
Final position	$\mathbf{p}_f$	$(0,1.5,1.5)$ m
Identified natural frequency	ω_n	3.2 rad/s
Identified damping ratio	ζ	0.063
Evaluation duration	T_e	15 s

4.5.2 Hardware Input Shaping Test

The hardware test compares the unshaped, ZV shaped, and ZVD shaped command cases under the same point-to-point motion. Figure 4.16 shows the corresponding y-direction command signals. The unshaped command changes directly from the initial command to the final command. In contrast, the ZV and ZVD commands distribute the change over delayed command components according to their impulse sequences. The ZVD command has the longest command duration because it uses an additional impulse compared with the ZV shaper.

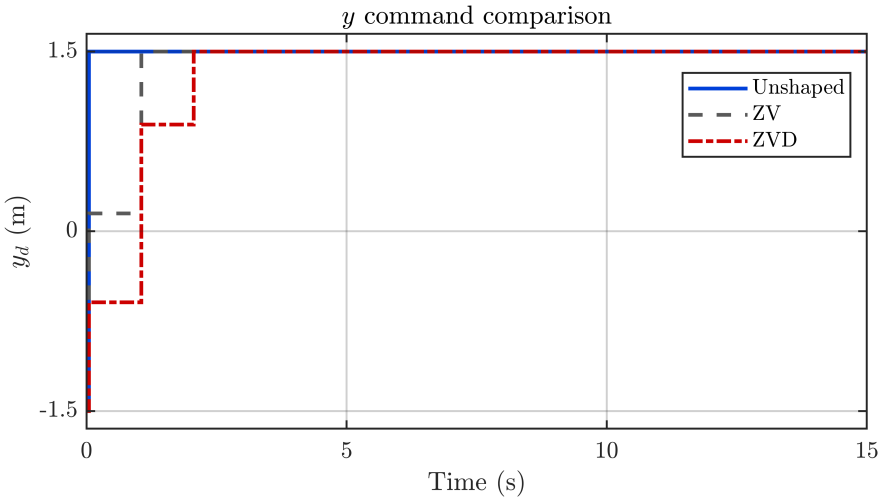

Figure 4.16: Experimental y-direction command comparison for the unshaped, ZV shaped, and ZVD shaped cases.

The corresponding y-position tracking responses are shown in Figure 4.17. All three cases reach the final commanded position. The unshaped command produces the fastest position transition, while the shaped commands result in smoother reference changes and slower position transitions. This behavior is expected because input shaping modifies the timing of the command before it is applied to the UAV position controller. The position tracking result also shows that the shaped commands do not prevent the UAV from reaching the final target position.

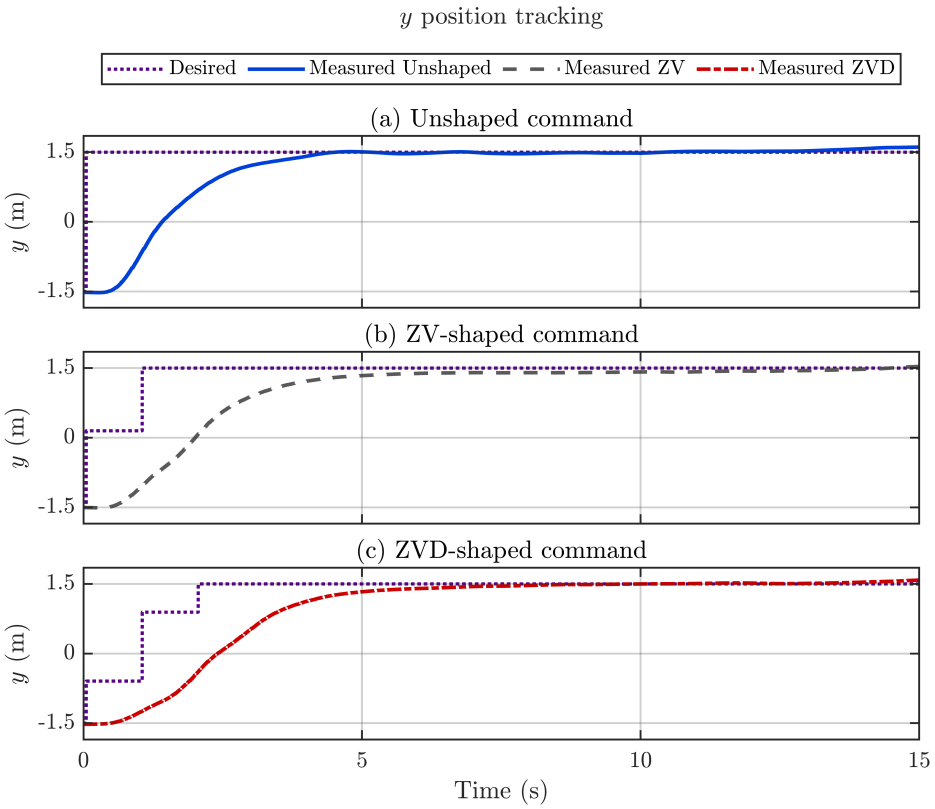

Figure 4.17: Experimental y-position tracking responses for the unshaped, ZV shaped, and ZVD shaped commands.

Figure 4.18 shows the measured payload swing angle θ_y for the three command cases. The unshaped command produces the largest payload oscillation because the direct command change strongly excites the suspended-payload mode. Both shaped commands

reduce the swing response compared with the unshaped case. The ZV shaper provides a clear reduction in the oscillation amplitude, while the ZVD shaper produces the smallest swing response over the test interval.

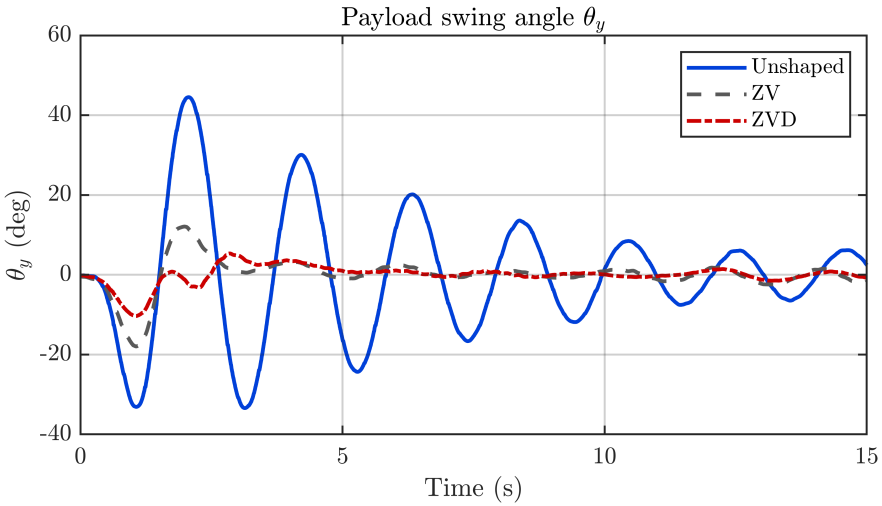

Figure 4.18: Experimental payload swing response θ_y for the unshaped, ZV shaped, and ZVD shaped commands.

The quantitative swing-angle metrics are summarized in Table 4.10. The unshaped command gives a maximum absolute swing angle of 44.52°, while the ZV shaper reduces it to 17.96°, corresponding to a reduction of approximately 59.7%. The ZVD shaper further reduces the maximum absolute swing angle to 10.35°, corresponding to a reduction of approximately 76.8%. The same trend is observed in the peak-to-peak, RMS, and MAE values. The RMS value decreases from 15.77° for the unshaped command to 4.24° for ZV and 2.45° for ZVD. These results show that the input shapers reduce both the peak swing response and the overall oscillatory content during the hardware test.

Table 4.10: Experimental swing-angle metrics for the hardware input shaping test.

Case	Max. $\lvert\theta_y\rvert$ (deg)	P–P θ_y (deg)	RMS θ_y (deg)	MAE θ_y (deg)
Unshaped	44.52	77.94	15.77	11.83
ZV	17.96	30.05	4.24	2.36
ZVD	10.35	15.69	2.45	1.46

4.5.3 Summary of Experimental Results

The hardware test verifies that the input shaping method reduces suspended-payload swing on the experimental UAV platform. For the fixed cable length of 1.0 m and payload mass of 0.2 kg, both shaped commands reduce the payload oscillation compared with the unshaped command. The ZV shaper reduces the maximum absolute swing angle from 44.52° to 17.96°, while the ZVD shaper further reduces it to 10.35°. This corresponds to reductions of approximately 59.7% and 76.8%, respectively.

The remaining swing metrics show the same trend. The RMS swing angle decreases from 15.77° for the unshaped command to 4.24° for the ZV shaped command and 2.45° for the ZVD shaped command. The peak-to-peak and MAE values are also reduced by both shapers, with the ZVD shaper producing the lowest values. These results confirm that the shaped commands reduce both the peak swing amplitude and the overall oscillatory content during the hardware test.

The experimental results are consistent with the simulation results presented earlier in this chapter. In both simulation and hardware testing, the ZV shaper provides swing reduction with a shorter command duration, while the ZVD shaper provides stronger attenuation. This agreement supports the use of input shaping as a feedforward swing-reduction method for suspended-payload transportation.

Overall, this chapter developed and evaluated the input shaping method used in the UAV suspended-payload system. The chapter introduced the suspended-payload model, formulated the ZV and ZVD shapers, described their implementation in the command architecture, and evaluated their performance in both simulation and hardware testing. The results show that input shaping can substantially reduce payload swing without requiring direct payload-swing feedback. Both of the simulation and hardware results demonstrate that input shaping provides an effective swing-reduction component

for suspended-payload motion. With this capability established, the following chapter considers how the developed system can be used within a broader mission scenario that includes obstacle-aware waypoint generation, cable adjustment, and water-sampling operation.

5 Application: Water Sampling

The previous chapters presented the main components of the UAV suspended-payload system, including the cable-adjustment mechanism, cable-length estimation, and input shaping for swing reduction. This chapter evaluates the integration of these components in a mission-level water sampling task. The purpose of this validation is to demonstrate that the proposed system can operate in constrained environments where direct flight to the target is not feasible and where the payload must be transported, lowered, and retrieved without requiring the UAV to land.

Water sampling is used in this chapter as a representative suspended-payload transportation application. The task requires the UAV to transport the payload through an obstacle-constrained environment, reach a target water tank, lower the payload into the water, collect a sample, retract the cable, and then move to a final position. This sequence combines the main functions developed in the thesis: suspended payload transportation, cable adjustment, swing reduction, and obstacle-aware waypoint generation.

Two different constrained mission scenarios are considered. Each scenario includes a different obstacle arrangement, gate configuration, and water tank location. For each scenario, a collision-free path is generated using a grid-based planner and then reduced to a smaller set of executable waypoints. The hardware mission is then conducted using both an unshaped command and a ZVD shaped command. This comparison is used to evaluate the effect of swing reduction on the overall mission execution, payload safety, and water collection performance.

5.1 Mission-Level Validation Overview

The mission-level validation is designed to evaluate the complete UAV suspended-payload framework in a constrained indoor environment. Unlike the point-to-point swing-reduction

tests presented in the previous chapter, the mission tests require the UAV to follow a sequence of waypoints, avoid obstacles, pass through constrained regions, and perform a payload operation at the water tank. Therefore, the mission validation provides a system-level evaluation rather than an isolated component test.

The overall mission consists of three main phases. In the first phase, the UAV transports the suspended payload from the start position toward the water sampling target while following the planned waypoint path. In the second phase, the UAV hovers above the target and adjusts the cable length to lower the payload into the water tank. Once the payload is submerged, water is collected passively through the open-top sampling container. In the third phase, the cable is retracted and the UAV continues to the final position.

During the transportation portions of the mission, the cable length is kept fixed and the UAV follows the planned waypoint sequence. Cable adjustment is performed while the UAV is hovering, which separates the lowering and retrieval operation from the translational motion. This operating procedure is consistent with the system design used in this thesis, where cable adjustment is used for the task operation and input shaping is used to reduce payload swing during fixed-length motion.

The two mission scenarios are used to evaluate the proposed framework under different constrained layouts. In both scenarios, the mission is performed once using the unshaped waypoint commands and once using ZVD shaped waypoint commands. The resulting payload swing metrics and water collection outcomes are then compared to assess the effect of input shaping on the complete mission.

5.2 Water Sampling Payload

A dedicated payload was designed for the water sampling task, as shown in Figure 5.1. The payload is 3D printed and is attached directly to the cable of the suspended-payload mechanism. The design uses an open-top container so that water can enter the payload

when it is lowered into the water tank. This passive sampling approach avoids the need for an additional pump, valve, or onboard sampling actuator.

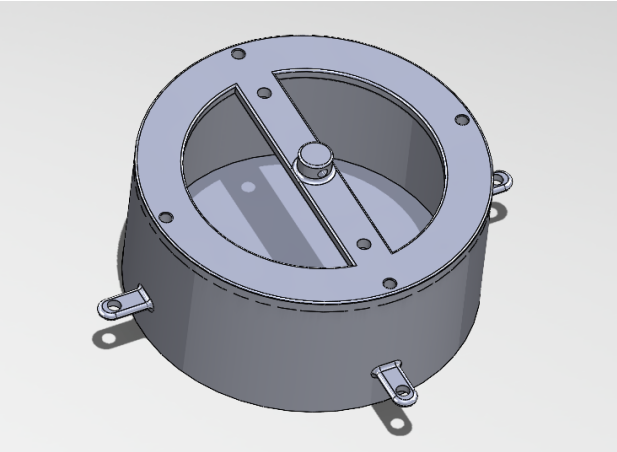

Figure 5.1: Designed water sampling payload used for the mission-level validation.

The payload is lowered into the tank by adjusting the cable length while the UAV is hovering above the target. After the payload is submerged and water is collected, the cable is retracted before the UAV continues to the next waypoint. This operation demonstrates the role of cable adjustment in extending the capability of the suspended-payload system beyond transportation alone. Instead of requiring the UAV to land near the water tank, the cable-adjustable mechanism allows the payload to interact with the target while the UAV remains above the constrained region.

5.3 Obstacle-Aware Mission Planning

An obstacle-Aware Mission Planning is used to generate waypoint paths for the constrained mission scenarios. The planner represents the indoor arena as a three-dimensional occupancy grid. The occupancy grid includes the arena boundaries, obstacle wall, gate structures, water tank, and safety margins associated with the UAV and suspended payload. The safety margins are included so that the planned path accounts for the physical size of the UAV, the payload, and expected tracking or swing deviations.

A grid-based A* search is used to generate the raw collision-free path between the mission points. A* is a heuristic graph-search method that evaluates nodes using a cost-to-come term and a heuristic cost-to-go term, allowing the search to be guided toward the goal while considering obstacle constraints. The algorithm was originally introduced by Hart, Nilsson, and Raphael and is widely used for path planning in grid-based environments [62]. In this work, the search is performed in the three-dimensional grid so that both horizontal position and altitude constraints can be considered.

The planner is applied in two stages. First, a raw path is generated from the start position to the water sampling target. Second, a second raw path is generated from the target position to the final position. These two path segments are then combined to form the complete mission path. The raw path typically contains many closely spaced grid points. Although this representation is suitable for search, it is not ideal for execution on the UAV because it creates an unnecessarily dense waypoint sequence.

To obtain a more practical waypoint sequence, a line-of-sight reduction step is applied after the raw path is generated. The reduction method checks whether non-adjacent points in the raw path can be connected directly without intersecting an occupied grid cell. If the direct connection is collision-free, the intermediate points are removed. This produces a shorter waypoint sequence while preserving obstacle clearance.

The output of the planning framework is a reduced waypoint path in the form

$$\mathbf{w}_i = \begin{bmatrix} x_i & y_i & z_i & \psi_i \end{bmatrix}, \tag{5.1}$$

where x_i, y_i, and z_i are the waypoint coordinates and ψ_i is the yaw command. In the implemented mission tests, the yaw command is kept fixed at zero. The reduced waypoint sequence is then sent to the UAV command-generation layer for mission execution. For the ZVD shaped case, the waypoint commands are shaped before being applied to the

UAV position-controller.

5.4 Mission Scenario 1

The first mission scenario evaluates the proposed system in a constrained environment where the UAV must transport the suspended payload to a water tank while avoiding obstacles. This scenario represents a water sampling task in which direct access to the target is restricted by the environment. Therefore, the UAV must follow an obstacle-aware waypoint path, reach the target region, lower the payload into the water using the cable-adjustment mechanism, collect water, retract the payload, and then continue to the final position.

Figure 5.2 shows the physical arena setup used for the first mission scenario. The setup includes the obstacle arrangement, gate structure, and water tank used as the sampling target. This physical layout was represented in the planner as a three-dimensional occupancy map that includes the obstacles, gate geometry, target location, and safety margins for the UAV and suspended payload.

The mission points for Scenario 1 are summarized in Table 5.1. The UAV starts at $(-1.4, -1.4, 1.6)$, moves to the water sampling target at $(0.6, 1.4, 1.0)$, and then continues to the final position at $(-1.4, 1.4, 1.0)$. During the main transportation portion of the mission, the cable length is 0.5 m. At the target, the UAV hovers above the water tank and the cable is released by approximately 0.3 m, increasing the cable length to 0.8 m so that the payload can enter the water. After sampling, the cable is retracted before the UAV continues to the final position.

Table 5.1: Mission points for scenario 1.

Point	x (m)	y (m)	z (m)	Yaw (rad)
Start	-1.4	-1.4	1.6	0
Target	0.6	1.4	1.0	0
Final	-1.4	1.4	1.0	0

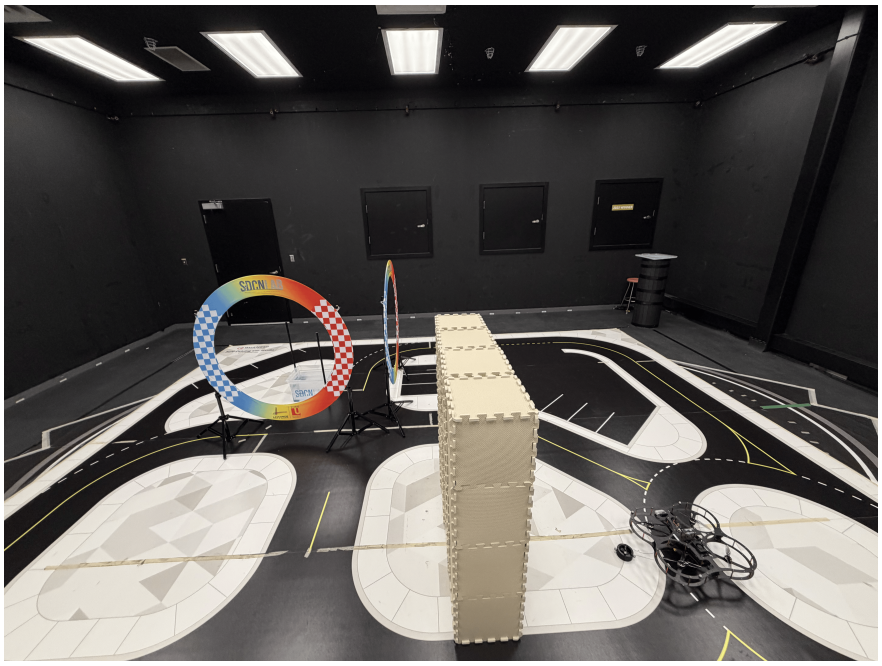

Figure 5.2: Physical arena setup for mission scenario 1.

The planner result for Scenario 1 is shown in Figure 5.3. The raw path generated by the A* search provides an obstacle-free path through the three-dimensional map. Since the raw path is generated on a discrete grid, it contains many closely spaced points. The line-of-sight reduction step is therefore applied to convert the raw path into a smaller set of executable waypoints while preserving collision-free connections between the remaining waypoints.

Figure 5.4 compares the raw A* path and the reduced waypoint path in the top view. The raw path contains 113 grid points, while the reduced path contains 7 executable waypoints. This reduction is important for hardware execution because it avoids sending an unnecessarily dense sequence of grid-level points to the UAV. The reduced waypoint path preserves the main obstacle-avoidance behavior while providing a compact command sequence for the mission controller.

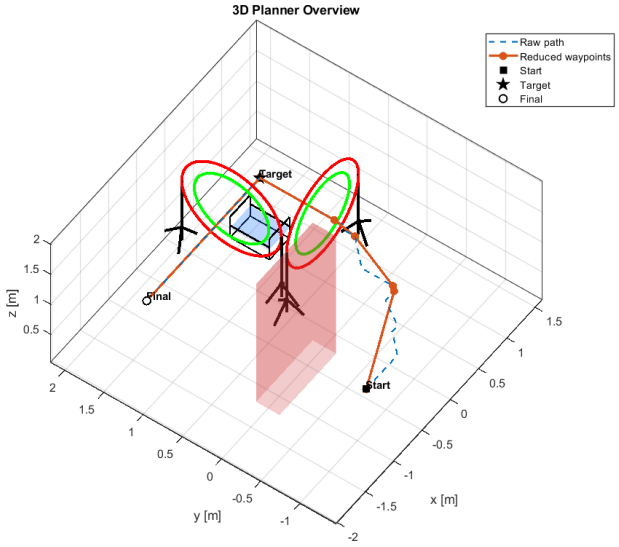

Figure 5.3: Three-dimensional planner result for mission scenario 1 showing the raw path and reduced waypoint path.

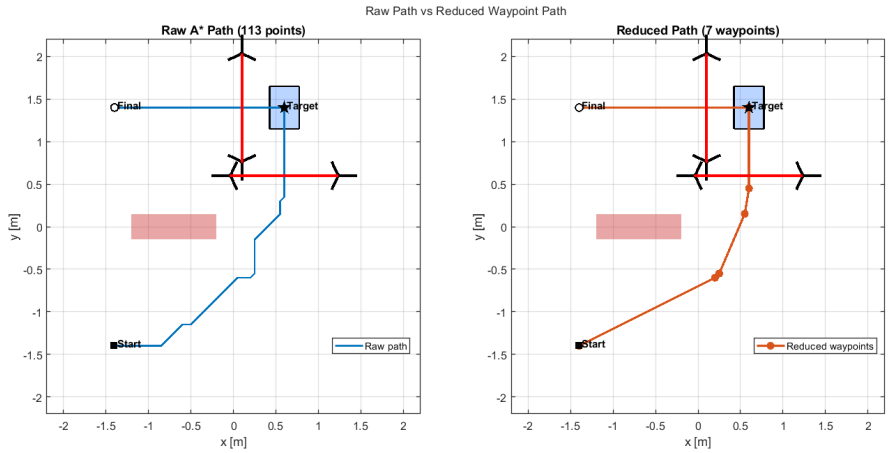

Figure 5.4: Raw A* path and reduced waypoint path for mission scenario 1.

The hardware mission was conducted using two command cases: an unshaped command and a ZVD shaped command. In both cases, the UAV followed the planned waypoint sequence and performed the water sampling operation. The unshaped mission was completed; however, the payload hit an obstacle during execution. In contrast, the ZVD shaped mission was completed safely, with reduced payload swing and without obstacle contact.

This comparison shows the importance of swing reduction when transporting a suspended payload in a constrained environment.

The swing-angle metrics for Scenario 1 are summarized in Table 5.2. The unshaped command produces a maximum swing angle of 47.745° in θ_x and 30.381° in θ_y. With the ZVD shaped command, these values are reduced to 12.368° and 7.1969°, respectively. This corresponds to reductions of approximately 74.1% in θ_x and 76.3% in θ_y. The peak-to-peak, RMS, and MAE values show the same trend, indicating that the ZVD shaped command reduces both the peak swing response and the overall oscillatory content over the full mission.

Table 5.2: Payload swing metrics for mission scenario 1.

Command case	Swing angle	Max. absolute angle (deg)	Peak-to-peak (deg)	RMS (deg)	MAE (deg)
Unshaped	θ_x	47.745	80.487	14.090	11.739
Unshaped	θ_y	30.381	55.167	9.4738	7.1867
ZVD shaped	θ_x	12.368	20.476	3.9336	3.0537
ZVD shaped	θ_y	7.1969	10.845	1.8428	1.2523

The water sampling result also improved when the ZVD shaped command was used. The unshaped mission collected approximately 90 g of water, while the ZVD shaped mission collected approximately 100 g. Although both missions completed the sampling sequence, the ZVD shaped command produced safer payload motion and improved the consistency of water collection.

5.5 Mission Scenario 2

The second mission scenario evaluates the proposed framework using a different constrained environment. This scenario changes the obstacle arrangement, gate location, and water tank location to test whether the mission-planning and water sampling approach can be adapted to another map. The objective is to validate the integrated system under a different constrained layout, rather than only repeating the same mithey mean the two

swing angles figureput the xyz coordinates nad ssion path.

Figure 5.5 shows the physical arena setup used for the second mission scenario. Similar to Scenario 1, the environment includes obstacles, a gate structure, and a water tank used as the sampling target. The physical environment was represented in the planner using a three-dimensional occupancy map that includes the main obstacle geometry, the gate constraint, the target region, and safety margins for the UAV and suspended payload.

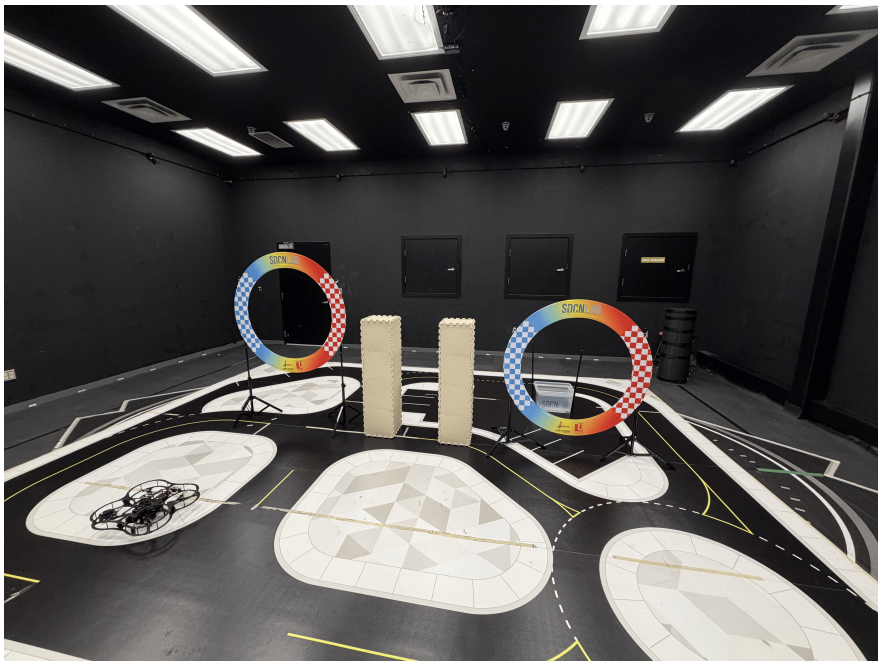

Figure 5.5: Physical arena setup for mission scenario 2.

The mission points for Scenario 2 are summarized in Table 5.3. The UAV starts at $(-1.4, 1.4, 1.6)$, moves to the water sampling target at $(0.6, -1.4, 1.0)$, and then continues to the final position at $(-1.4, 0, 1.0)$. In this scenario, the cable length is initially 0.7 m. Before passing through the gate, the cable is adjusted to 0.5 m to satisfy the gate-clearance requirement. At the water sampling target, the cable is then released by approximately 0.3 m so that the payload can enter the water. After sampling, the cable is retracted before the UAV continues to the final position.

Table 5.3: Mission points for scenario 2.

Point	x (m)	y (m)	z (m)	Yaw (rad)
Start	-1.4	1.4	1.6	0
Target	0.6	-1.4	1.0	0
Final	-1.4	0.0	1.0	0

The three-dimensional planner result for Scenario 2 is shown in Figure 5.6. The planner generates an obstacle-free path from the start position to the water sampling target and then to the final position. The path passes through the feasible region of the environment while avoiding the occupied regions represented in the occupancy grid.

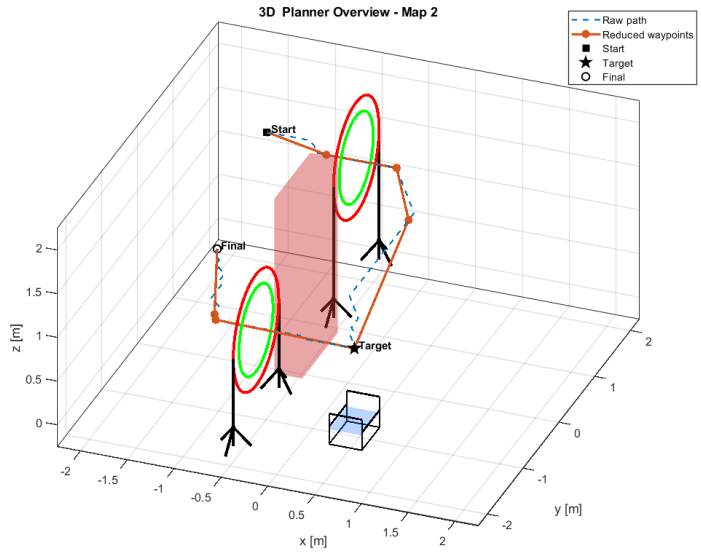

Figure 5.6: Three-dimensional planner result for mission scenario 2 showing the raw path and reduced waypoint path.

Figure 5.7 compares the raw A* path and the reduced waypoint path for Scenario 2. The raw path contains 141 grid points, while the reduced path contains 8 executable waypoints. As in Scenario 1, the line-of-sight reduction step reduces the number of waypoints while preserving the main obstacle-avoidance behavior of the planned path. This produces a compact waypoint sequence suitable for the hardware mission.

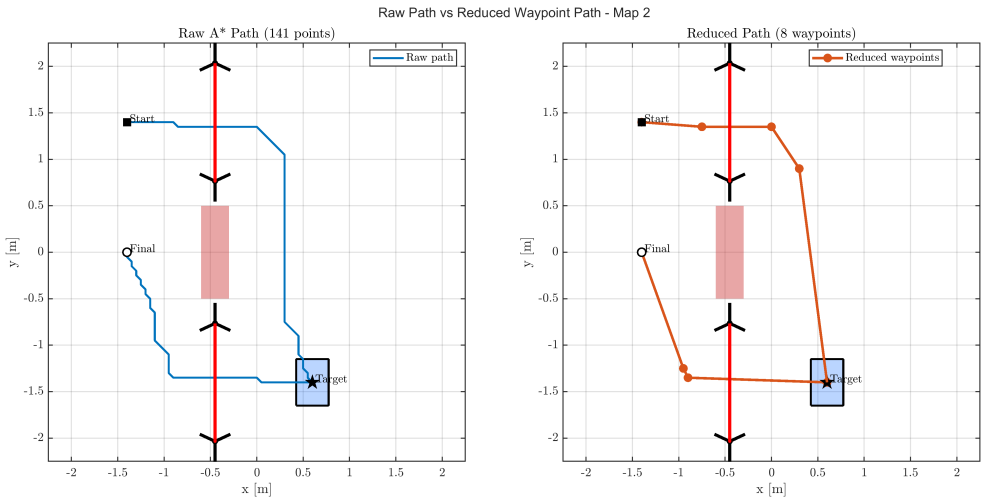

Figure 5.7: Raw A* path and reduced waypoint path for mission scenario 2.

The hardware mission for Scenario 2 was also conducted using both unshaped and ZVD shaped commands. The unshaped mission was completed; however, the payload hit the water tank during execution. The ZVD shaped mission was completed safely, with reduced payload swing and without obstacle contact. This result further shows that swing reduction is important for suspended-payload transportation in constrained environments, especially when the payload must pass near obstacles or through restricted regions.

The swing-angle metrics for Scenario 2 are summarized in Table 5.4. In the unshaped case, the maximum swing angle reaches 38.433° in θ_x and 67.036° in θ_y. With the ZVD shaped command, these values are reduced to 8.8817° and 18.244°, respectively. This corresponds to reductions of approximately 76.9% in θ_x and 72.8% in θ_y. The RMS and MAE values also decrease substantially, indicating that the ZVD shaped command reduces both large swing peaks and sustained oscillations during the complete mission.

The water sampling result follows the same trend observed in Scenario 1. The unshaped mission collected approximately 90 g of water, while the ZVD shaped mission collected approximately 100 g. The improved result with ZVD indicates that reducing payload swing helps the passive open-top sampling payload enter and leave the water

more consistently during the mission.

Table 5.4: Payload swing metrics for mission scenario 2.

Command case	Swing angle	Max. absolute angle (deg)	Peak-to-peak (deg)	RMS (deg)	MAE (deg)
Unshaped	θ_x	38.433	68.193	13.076	10.827
Unshaped	θ_y	67.036	113.82	24.854	20.698
ZVD shaped	θ_x	8.8817	17.524	2.7770	2.1847
ZVD shaped	θ_y	18.244	30.602	5.8587	3.8634

5.6 Mission-Level Results and Discussion

The results from the two mission scenarios demonstrate that the proposed UAV suspended-payload system can perform the considered water lets move on sampling missions within the controlled indoor constrained environments used in this study. In both scenarios, the planner generated an obstacle-free raw path through the three-dimensional map, and the line-of-sight reduction step converted the dense raw path into a smaller set of executable waypoints. In Scenario 1, the raw path was reduced from 113 grid points to 7 waypoints. In Scenario 2, the raw path was reduced from 141 grid points to 8 waypoints. This reduction preserved the main obstacle-avoidance behavior while producing a practical waypoint sequence for hardware execution.

The mission results also show that the ZVD shaped command improved the suspended-payload behavior compared with the unshaped command. In both scenarios, the unshaped mission was completed, but the payload hit an obstacle during execution. In contrast, the ZVD shaped mission was completed safely in both scenarios. This difference highlights the importance of swing reduction in constrained suspended-payload transportation. Even when the UAV follows an obstacle-free path, the suspended payload can deviate from the UAV trajectory because of oscillatory motion. Therefore, reducing payload swing is important for maintaining clearance between the payload and nearby obstacles.

Table 5.5 summarizes the reduction in maximum absolute payload swing angle ob-

tained using ZVD shaping. In Scenario 1, the ZVD shaped command reduces the maximum θ_x swing by approximately 74.1% and the maximum θ_y swing by approximately 76.3%. In Scenario 2, the corresponding reductions are approximately 76.9% and 72.8%. These results show that the ZVD shaper remains effective during mission-level execution, where the UAV follows multiple waypoint segments and performs a sampling operation rather than a single isolated point-to-point motion.

Table 5.5: Reduction in maximum absolute payload swing angle using ZVD shaping.

Scenario	Reduction in max. $\lvert\theta_x\rvert$	Reduction in max. $\lvert\theta_y\rvert$
1	74.1%	76.3%
2	76.9%	72.8%

The water collection results are summarized in Table 5.6. In both mission scenarios, the unshaped command collected approximately 90 g of water, while the ZVD shaped command collected approximately 100 g. Since the water sampling payload is a passive open-top container, the collected amount depends on how consistently the payload enters the water and how much unwanted motion occurs during the sampling operation. The improved water collection in the ZVD shaped missions indicates that reducing payload swing contributes not only to safer obstacle clearance but also to more consistent task execution.

Table 5.6: Water collection results for the two mission scenarios.

Scenario	Unshaped command	ZVD shaped command
1	90 g	100 g
2	90 g	100 g

The mission tests also demonstrate the role of cable adjustment in the proposed framework. The UAV did not need to land near the water tank to complete the sampling task. Instead, the payload was lowered into the water while the UAV hovered above the target region, and the cable was retracted before the UAV continued to the final position. This capability is important for constrained or hard-to-access environments, where landing

near the target may be unsafe or infeasible.

Overall, the mission-level results show that the proposed framework can combine obstacle-aware mission planning, cable-adjustable payload operation, and ZVD input shaping to complete a constrained water sampling task. The planner provides feasible waypoint sequences, the cable-adjustment mechanism enables payload lowering and retrieval, and input shaping improves payload safety and task consistency during the mission. The complete water-sampling mission is shown in an online supplementary video: water sampling mission demonstration.

5.7 Summary

This chapter presented the water sampling validation of the UAV suspended-payload system. The objective was to evaluate the complete framework in constrained mission scenarios, rather than only testing the individual components separately. A passive open-top water sampling payload was used as the application payload, and two different obstacle-constrained maps were considered for hardware validation.

An obstacle-aware mission-planning framework was used to generate feasible waypoint paths for both scenarios. The planner first generated a raw path using a grid-based A* search in a three-dimensional occupancy map. A line-of-sight waypoint reduction step was then applied to reduce the raw path into a smaller number of executable waypoints. This produced practical waypoint sequences for the QDrone2 while preserving the main obstacle-avoidance behavior required for the mission.

The two hardware mission scenarios were executed using both unshaped and ZVD shaped waypoint commands. In both scenarios, the unshaped mission was completed, but the payload hit an obstacle during execution. In contrast, the ZVD shaped mission was completed safely. The swing-angle metrics showed that ZVD input shaping substantially reduced the payload swing over the full mission. The reduction in maximum swing angle

was greater than 70% in both swing directions for both mission scenarios.

The water collection results also improved when ZVD input shaping was used. In both scenarios, the unshaped command collected approximately 90 g of water, while the ZVD shaped command collected approximately 100 g. This result indicates that reducing payload swing improves not only obstacle clearance but also the consistency of the water sampling operation.

Overall, the results in this chapter validate the integrated UAV suspended-payload framework developed in this thesis. The mission experiments demonstrate that the proposed system can combine obstacle-aware waypoint generation, cable-adjustable payload operation, and input shaped motion commands to perform constrained water sampling missions with improved payload behavior and safer task execution.

6 Conclusion and Future Work

6.1 Conclusion

This thesis developed a cable-adjustable UAV suspended-payload system for constrained transportation applications. The work was motivated by the need for UAV systems that can transport and interact with payloads in locations where landing is unsafe, infeasible, or restricted by the environment. A suspended-payload configuration allows the UAV to remain above the target region while the payload is lowered to perform the task. However, this configuration introduces two main challenges: the payload must be positioned at different vertical distances from the UAV, and payload swing must be reduced during transportation to improve safety and task reliability.

To address the first challenge, a cable-adjustment mechanism was designed, fabricated, and integrated with the Quanser QDrone2 platform. The mechanism allows the payload to be released and retracted without requiring a separate onboard power system or additional complex electronics. A command-based cable-length estimation method was also developed to estimate the cable length from the known initial length and the commanded motor actuation time. This approach avoids the need for a direct cable-length sensor while still providing sufficient cable-length awareness for the experimental missions considered in this thesis. Cable adjustment was performed during hovering, while translational motion was carried out with a fixed cable length.

To address the second challenge, input shaping was implemented as a feedforward swing-reduction method. The suspended payload was modeled as a cable-dependent oscillatory system, and ZV and ZVD input shapers were parameterized based on the payload swing dynamics. Input shaping was selected because it can reduce payload oscillation by modifying the reference command before it reaches the existing UAV position-controller, without requiring direct payload-swing feedback. Simulation results

showed that both ZV and ZVD input shaping reduced payload swing compared with the unshaped command, with ZVD providing stronger attenuation and improved robustness to natural-frequency variation.

The input shaping method was then validated experimentally using the UAV suspended-payload platform. In the hardware test with a 1.0 m cable length and a 0.2 kg payload, the ZV and ZVD commands both reduced the measured payload swing compared with the unshaped command. The maximum absolute swing angle in the y-direction was reduced from 44.52° for the unshaped command to 17.96° with ZV and 10.35° with ZVD. The RMS and MAE values followed the same trend, confirming that input shaping reduced both the peak swing and the overall oscillatory content during hardware flight.

Finally, the complete system was evaluated through mission-level water sampling experiments in two constrained maps. A grid-based A* planner was used to generate obstacle-free raw paths, and a line-of-sight waypoint reduction step was applied to convert the dense raw paths into shorter executable waypoint sequences. The missions integrated the cable-adjustment mechanism, suspended-payload transportation, ZVD shaped waypoint motion, and passive water collection using a 3D-printed open-top sampling payload. In both scenarios, the unshaped missions were completed but the payload hit an obstacle during execution, while the ZVD-shaped missions were completed safely. The ZVD-shaped missions also reduced the maximum payload swing by more than 70% in both swing directions and increased the collected water from approximately 90 g to 100 g.

Overall, the results demonstrate that the cable-adjustment mechanism, command-based cable-length estimation, feedforward swing reduction, and obstacle-aware mission planning can be integrated into a functional UAV suspended-payload system under the controlled indoor conditions considered in this work. The thesis shows that water sampling can be used as a representative application to validate the complete system, where the payload must be transported, lowered, retrieved, and safely moved through a constrained

environment. The experimental results support the effectiveness of the developed system and show that ZVD input shaping improves both payload safety and task consistency during mission-level operation.

6.2 Limitations

The experimental validation in this thesis was conducted in a controlled indoor laboratory environment using OptiTrack motion capture and predefined static obstacle maps. Therefore, the reported results represent the tested indoor conditions and do not directly establish performance under outdoor environmental effects such as wind, precipitation, temperature variation, or unknown and changing obstacles. Water sampling was used as the mission-level validation application, and application of the framework to other suspended-payload tasks would require additional application-specific validation.

The cable-adjustment system uses an open-loop command-based method rather than direct cable-length feedback. The cable length is inferred from the known initial length and experimentally calibrated motor command duration, and small differences between commanded and achieved cable lengths may occur because of cable winding, friction, tension, spool effects, and actuator variation. The validation results in this thesis quantify the performance of this method under the tested hardware and operating conditions.

The ZV and ZVD input shapers are feedforward command filters parameterized using the identified dominant payload swing dynamics. Cable length is kept fixed during translational motion, while cable adjustment is performed during hovering phases. Because payload swing is not directly measured by the shaper, disturbances or substantial changes in the identified system dynamics may reduce swing-reduction performance compared with the controlled conditions evaluated in this thesis.

6.3 Future Work

Several directions can be considered to extend the work presented in this thesis. First, the input shaping method can be extended to account for cable-length variation in more complex missions. In the current implementation, cable adjustment was performed while the UAV was hovering, and input shaping was applied during fixed-length translational motion. Future work could investigate adaptive or online input shaping so that the shaper parameters are updated automatically when the cable length changes. This would allow the swing-reduction method to be applied more flexibly in missions involving multiple payload heights or repeated changes in cable length.

Second, the mission-planning framework can be extended from predefined maps to perception-based or online planning. The planner used in this thesis relied on a known representation of the environment. Future work could integrate onboard perception, map updating, or obstacle detection so that the UAV can adapt to changes in the environment during operation. This would make the system more suitable for less controlled environments where obstacle locations may not be known in advance.

Overall, these future directions would extend the present work while preserving the main framework developed in this thesis. The results of this research demonstrate that a cable-adjustable mechanism, command based cable-length awareness, input shaped motion commands, and obstacle-aware mission planning can be integrated into a functional UAV suspended-payload system. Future extensions can build on this foundation to increase autonomy, scalability, and robustness, while maintaining the practical advantages of the proposed reduced sensing approach.

Bibliography

[1] M. Bernard, K. Kondak, I. Maza, and A. Ollero, "Autonomous transportation and deployment with aerial robots for search and rescue missions," *Journal of Field Robotics*, vol. 28, no. 6, pp. 914–931, 2011.

[2] N. Michael, J. Fink, and V. Kumar, "Cooperative manipulation and transportation with aerial robots," *Autonomous Robots*, vol. 30, pp. 73–86, 2011.

[3] J. Estevez, G. Garate, J. M. Lopez-Guede, and M. Larrea, "Review of aerial transportation of suspended-cable payloads with quadrotors," *Drones*, vol. 8, no. 2, p. 35, 2024.

[4] S. Tang, V. Wüest, and V. Kumar, "Aggressive flight with suspended payloads using vision-based control," *IEEE Robotics and Automation Letters*, vol. 3, no. 2, pp. 1152–1159, 2018.

[5] G. Li, A. Tunchez, and G. Loianno, "PCMPC: Perception-constrained model predictive control for quadrotors with suspended loads using a single camera and IMU," in *Proceedings of the 2021 IEEE International Conference on Robotics and Automation (ICRA)*, pp. 2012–2018, 2021.

[6] S. Li and L. Feng, "Energy-efficiency-oriented vision feedback control of qcsp systems: Linear adrc approach," *Frontiers in Energy Research*, vol. 10, p. 865069, 2022.

[7] S. Wang, H. Chen, J. Liu, and Y. Liu, "Adaptive trajectory tracking of uav with a cable-suspended load using vision-inertial-based estimation," *Automatica*, vol. 158, p. 111310, 2023.

[8] K. Sreenath, N. Michael, and V. Kumar, "Trajectory generation and control of a quadrotor with a cable-suspended load: A differentially-flat hybrid system," in *Proceedings of the IEEE International Conference on Robotics and Automation*, pp. 4888–4895, 2013.

[9] I. Palunko, R. Fierro, and P. Cruz, "Trajectory generation for swing-free maneuvers of a quadrotor with suspended payload: A dynamic programming approach," in *Proceedings of the IEEE International Conference on Robotics and Automation*, pp. 2691–2697, 2012.

[10] S. Tang and V. Kumar, "Mixed integer quadratic program trajectory generation for a quadrotor with a cable-suspended payload," in *Proceedings of the IEEE International Conference on Robotics and Automation*, pp. 2216–2222, 2015.

[11] P. Foehn, D. Falanga, N. Kuppuswamy, R. Tedrake, and D. Scaramuzza, "Fast trajectory optimization for agile quadrotor maneuvers with a cable-suspended payload," in *Robotics: Science and Systems*, 2017.

[12] J. Zeng, P. Kotaru, M. W. Mueller, and K. Sreenath, "Differential flatness based path planning with direct collocation on hybrid modes for a quadrotor with a cable-suspended payload," *IEEE Robotics and Automation Letters*, vol. 5, no. 2, pp. 3074–3081, 2020.

[13] N. C. Singer and W. P. Seering, "Preshaping command inputs to reduce system vibration," *Journal of Dynamic Systems, Measurement, and Control*, vol. 112, no. 1, pp. 76–82, 1990.

[14] W. Singhose, "Command shaping for flexible systems: A review of the first 50 years," *International Journal of Precision Engineering and Manufacturing*, vol. 10, no. 4, pp. 153–168, 2009.

[15] C. Koparan, A. B. Koc, C. V. Privette, C. B. Sawyer, and J. L. Sharp, "Evaluation of a uav-assisted autonomous water sampling," *Water*, vol. 10, no. 5, p. 655, 2018.

[16] J. H. Ryu, "Uas-based real-time water quality monitoring, sampling, and visualization platform," *Sensors*, 2022.

[17] R. Zhang *et al.*, "Water quality sampling and multi-parameter monitoring system based on a multi-rotor unmanned aerial vehicle," *Water*, vol. 15, no. 11, p. 2129, 2023.

[18] F. Panetsos, G. C. Karras, and S. Aspragkathos, "Precise position control of a multirotor uav with a cable-suspended mechanism during water sampling," in *Proceedings of the IEEE/RSJ International Conference on Intelligent Robots and Systems*, 2022.

[19] F. Panetsos, G. C. Karras, K. J. Kyriakopoulos, *et al.*, "A motion control framework for autonomous water sampling and swing-free transportation of a multirotor uav with a cable-suspended mechanism," *Journal of Field Robotics*, vol. 40, no. 5, pp. 1209–1230, 2023.

[20] Google, "Gemini photos." `https://gemini.google.com/`, July 2026.

[21] Mr. Wang, "How drone water sampling is transforming water quality monitoring." `https://www.vastarrive.com/drone-water-sampling-for-water-quality-monitoring`, July 2026.

[22] K. Sreenath and V. Kumar, "Dynamics, control and planning for cooperative manipulation of payloads suspended by cables from multiple quadrotor robots," in *Robotics: Science and Systems*, 2013.

[23] H. Alkomy and J. Shan, "Vibration reduction of a quadrotor with a cable-suspended payload using polynomial trajectories," *Nonlinear Dynamics*, vol. 104, no. 4, pp. 3713–3735, 2021.

[24] A. Akhtar, S. Saleem, and J. Shan, "Path invariant controllers for a quadrotor with a cable-suspended payload using a global parameterization," *IEEE Transactions on Control Systems Technology*, vol. 30, no. 5, pp. 2002–2017, 2022.

[25] A. Akhtar, S. Saleem, and J. Shan, "Path following of a quadrotor with a cable-suspended payload," *IEEE Transactions on Industrial Electronics*, vol. 70, no. 2, pp. 1646–1654, 2023.

[26] J. Kang, J. Shan, and H. Alkomy, "Control framework for a UAV slung-payload transportation system," *IEEE Control Systems Letters*, vol. 7, pp. 2473–2478, 2023.

[27] H. Li, H. Wang, C. Feng, F. Gao, B. Zhou, and S. Shen, "AutoTrans: A complete planning and control framework for autonomous UAV payload transportation," *IEEE Robotics and Automation Letters*, vol. 8, no. 10, pp. 6859–6866, 2023.

[28] K. Sreenath, T. Lee, and V. Kumar, "Geometric control and differential flatness of a quadrotor UAV with a cable-suspended load," in *Proceedings of the 52nd IEEE Conference on Decision and Control*, pp. 2269–2274, 2013.

[29] X. Liang, Y. Fang, N. Sun, and H. Lin, "Nonlinear hierarchical control for unmanned quadrotor transportation systems," *IEEE Transactions on Industrial Electronics*, vol. 65, no. 4, pp. 3395–3405, 2018.

[30] J. Kang and J. Shan, "Coupling-enhanced smooth adaptive control for underactuated UAV-slung-payload systems," *IEEE/ASME Transactions on Mechatronics*, vol. 30, no. 6, pp. 7066–7076, 2025.

[31] J. Kang and J. Shan, "Virtual nonholonomic constraints-based motion control for underactuated UAV slung-payload systems," *IEEE Transactions on Automatic Control*, vol. 70, no. 10, pp. 7047–7054, 2025.

[32] F. A. Goodarzi, D. Lee, and T. Lee, "Geometric control of a quadrotor UAV transporting a payload connected via flexible cable," *International Journal of Control, Automation and Systems*, vol. 13, no. 6, pp. 1486–1498, 2015.

[33] J. Kang and J. Shan, "Trajectory planning for UAV transportation systems using RRT*-informed NMPC," in *Proceedings of the 2024 IEEE International Conference on Systems, Man, and Cybernetics (SMC)*, pp. 994–998, 2024.

[34] A. Faust, I. Palunko, P. Cruz, R. Fierro, and L. Tapia, "Learning swing-free trajectories for UAVs with a suspended load," in *Proceedings of the IEEE International Conference on Robotics and Automation*, pp. 4902–4909, 2013.

[35] M. M. Nicotra, E. Garone, R. Naldi, and L. Marconi, "Nested saturation control of an UAV carrying a suspended load," in *Proceedings of the American Control Conference*, pp. 3585–3590, 2014.

[36] M. E. Guerrero, D. A. Mercado, R. Lozano, and C. D. García, "Passivity based control for a quadrotor UAV transporting a cable-suspended payload with minimum swing," in *Proceedings of the 54th IEEE Conference on Decision and Control*, pp. 6718–6723, 2015.

[37] M. E. Guerrero-Sánchez, D. A. Mercado-Ravell, R. Lozano, and C. D. García-Beltrán, "Swing-attenuation for a quadrotor transporting a cable-suspended payload," *ISA Transactions*, vol. 68, pp. 433–449, 2017.

[38] J. Kang, J. Shan, and H. Alkomy, "VNHC-based continuous sliding mode control for an underactuated tethered UAV system," *IEEE Transactions on Industrial Electronics*, 2024. Early Access.

[39] Y. Zhu, Z. Zheng, J. Shao, H. Huang, and W. Xing Zheng, "Modeling, robust control design, and experimental verification for quadrotor carrying cable-suspended payload," *IEEE Transactions on Automation Science and Engineering*, vol. 22, pp. 6061–6075, 2024.

[40] K. Zhao, G. Wang, J. Cai, and B. Xian, "Antiswing control strategy for quadrotor transporting a cable-suspended payload: A two-stage ADRC approach," *IEEE/ASME Transactions on Mechatronics*, 2024.

[41] S. Sadr, S. A. A. Moosavian, and P. Zarafshan, "Dynamics and command shaping control of quadcopters carrying suspended loads," in *IFAC-PapersOnLine*, vol. 51, pp. 474–479, 2018.

[42] C. Li, X. Huo, and Q. Liu, "A new robust command shaping method and its application in quadrotor slung system with varying parameters," *IFAC-PapersOnLine*, vol. 53, no. 2, pp. 5737–5742, 2020.

[43] J. B. Ubbink and J. A. A. Engelbrecht, "Sequence-constrained trajectory planning and execution for a quadrotor UAV with suspended payload," *IFAC-PapersOnLine*, vol. 53, no. 2, pp. 9405–9411, 2020.

[44] I. Palunko, A. Faust, P. Cruz, L. Tapia, and R. Fierro, "A reinforcement learning approach towards autonomous suspended load manipulation using aerial robots," in *Proceedings of the IEEE International Conference on Robotics and Automation*, pp. 4896–4901, 2013.

[45] J. Potter, W. Singhose, and M. Costello, "Reducing swing of model helicopter sling load using input shaping," in *Proceedings of the IEEE International Conference on Control and Automation*, pp. 348–353, 2011.

[46] C. Adams, J. Potter, and W. Singhose, "Input-shaping and model-following control of a helicopter carrying a suspended load," *Journal of Guidance, Control, and Dynamics*, vol. 38, no. 1, pp. 94–105, 2015.

[47] J. J. Potter, C. J. Adams, and W. Singhose, "A planar experimental remote-controlled helicopter with a suspended load," *IEEE/ASME Transactions on Mechatronics*, vol. 20, no. 5, pp. 2496–2503, 2015.

[48] P. Homolka, M. Hromcik, and T. Vyhlidal, "Input shaping solutions for drones with suspended load: First results," in *Proceedings of the 21st International Conference on Process Control*, 2017.

[49] S. Fielding and M. A. Nahon, "Input shaped trajectory generation and controller design for a quadrotor-slung load system," in *Proceedings of the 2019 International Conference on Unmanned Aircraft Systems (ICUAS)*, pp. 162–170, 2019.

[50] X. Huo, J. Chen, Q. Liu, and X. He, "Vibration elimination for quadrotor slung system based on input shaping and double closed-loop control," in *Proceedings of the 12th Asian Control Conference*, pp. 492–497, 2019.

[51] O. Ogunbodede and T. Singh, "Load vibration mitigation in unmanned aerial vehicles with cable suspended load," *Journal of Autonomous Vehicles and Systems*, vol. 1, no. 3, p. 034502, 2021.

[52] Z. Li, J. C. Erskine, S. Caro, and A. Chriette, "Design and control of a variable aerial cable towed system," *IEEE Robotics and Automation Letters*, vol. 5, no. 2, pp. 636–643, 2020.

[53] Y. Yang, Y. Hu, S. Li, and D. Zhang, "Anti-swing control and trajectory planning of quadrotor suspended payload system with variable length cable," *Asian Journal of Control*, vol. 24, no. 5, pp. 2424–2436, 2022.

[54] Y. S. Sarkisov, A. Coelho, M. G. Santos, M. J. Kim, D. Tsetserukou, C. Ott, and K. Kondak, "Hierarchical whole-body control of the cable-suspended aerial manipulator endowed with winch-based actuation," in *Proceedings of the 2023 IEEE International Conference on Robotics and Automation (ICRA)*, pp. 5366–5372, 2023.

[55] S. Li, T. T. H. Duong, and D. Zanotto, "In-flight cable length control for improved quadrotor-based suspended load transportation," *IEEE Robotics and Automation Letters*, vol. 9, no. 1, pp. 667–674, 2024.

[56] D. Zhang, H. Han, Y. Yang, and Y. Hu, "Modeling and anti-swing control of quadrotor-suspended system with variable cable length at unequal speed," *Transactions of the Institute of Measurement and Control*, vol. 46, no. 6, pp. 1177–1189, 2024.

[57] F. A. Goodarzi, "Autonomous aerial payload delivery with quadrotor using varying length cable," in *Proceedings of the 2016 International Conference on Advanced Mechatronic Systems*, (Melbourne, Australia), pp. 394–399, 2016.

[58] J.-P. Ore, S. Elbaum, A. Burgin, and C. Detweiler, "Autonomous aerial water sampling," *Journal of Field Robotics*, vol. 32, no. 8, pp. 1095–1113, 2015.

[59] Quanser Inc., "QDrone 2." `https://www.quanser.com/products/qdrone-2/`, 2026. Accessed: 2026-02-05.

[60] NaturalPoint, Inc., "OptiTrack Flex 13 camera." `https://old.optitrack.com/cameras/flex-13/buy.html`, 2026. Accessed: 2026-02-05.

[61] NaturalPoint, Inc., "OptiTrack precision capture quick start guide." https://docs.optitrack.com/quick-start-guides/quick-start-guide-precision-capture, 2026. Accessed: 2026-02-05.

[62] P. E. Hart, N. J. Nilsson, and B. Raphael, "A formal basis for the heuristic determination of minimum cost paths," *IEEE Transactions on Systems Science and Cybernetics*, vol. 4, no. 2, pp. 100–107, 1968.